Nonthermal radiative transfer of oxygen 98.9 nm ultraviolet emission : solving an old mystery.

B. Hubert[(1)], J.C. Gérard[(1)], V.I. Shematovich[(2)], D.V. Bisikalo[(2)], S. Chakrabarti[(3)], G.R. Gladstone[(4)]

1. Laboratory for Planetary and Atmospheric Physics (LPAP), University of Liège, Liège, Belgium
2. Institute of Astronomy of the Russian Academy of Sciences, Moscow, Russia
3. Lowell Center for Space Science and Technology, University of Massachusetts, MA, USA.
4. Southwest Research Institute, San Antonio, TX, USA

Please cite as:

Hubert, B., J.-C. Gérard, V. I. Shematovich, D. V. Bisikalo, S. Chakrabarti, and G. R. Gladstone (2015), Nonthermal radiative transfer of oxygen 98.9 nm ultraviolet emission: Solving an old mystery, J. Geophys. Res. Space Physics, 120, doi:10.1002/2014JA020835.

Journal of Geophysical Research

Accepted November 2015

Abstract

Sounding rocket measurements conducted in 1988 under high solar activity conditions revealed that the intensity of thermospheric OI emissions at 98.9 nm present an anomalous vertical profile, showing exospheric intensities much higher than expected from radiative transfer model results, which included the known sources of excited oxygen. All attempts based on modeling of the photochemical processes and radiative transfer were unable to account for the higher than predicted brightnesses. More recently, the SOHO-SUMER instrument measured the UV solar flux at high spectral resolution, revealing the importance of a significant additional source of oxygen emission at 98.9 nm that had not been accounted for before. In this study, we simulate the radiative transfer of the OI-98.9 nm multiplet, including the photochemical sources of excited oxygen, the resonant scattering of solar photons, and the effects of non-thermal atoms, i.e. a population of fast-moving oxygen atoms in excess of the Maxwellian distribution. Including resonance scattering of the 98.9 nm solar multiplet, we find good agreement with the previous sounding rocket observation. The inclusion of a nonthermal oxygen population with a consistent increase of the total density produces a larger intensity at high altitude that apparently better accounts for the observation, but such a correction cannot be demonstrated given the uncertainties of the observations. A good agreement between model and sounding rocket observation is also found with the triplet at 130.4 nm. We further investigate the radiative transfer of the OI-98.9 nm multiplet, and the oxygen emissions at 130.4 and 135.6 nm using observations from the STP78-1 satellite. We find a less satisfying agreement between the model and the STP78-1 data that can be accounted for by scaling the modelled intensity within a range acceptable given the uncertainties on the STP78-1 absolute calibration.

1. Introduction

The photochemistry of thermospheric oxygen includes several exothermal reactions that produce ground state oxygen atoms $O(^3P)$ with a large kinetic energy compared with the average thermal energy of the thermosphere. For example, photodissociation of O_2 and dissociative recombination of O_2^+ ions release fast $O(^3P)$ atoms with an exothermicity that depends on the excitation state of the produced oxygen. Kella et al. [1997] studied the dissociative recombination of O_2^+ and determined the branching ratios of the different reaction products. Several exothermic reactions were also given by Rees [1989] and Roble [1995], and the most important exothermal processes relevant to the oxygen photochemistry are listed with their exothermicity and reaction parameter in **Table 1**, after Richards et al. [1994a].

In the upper thermosphere, and, in particular, the exosphere, the frequency of collisions between particles dramatically decreases with increasing altitude, along with the exponentially decreasing gas density. As a result, thermalization of $O(^3P)$ atoms produced by exothermal processes becomes less efficient, and a significant population with large kinetic energy can exist in addition to the high energy tail of the Maxwellian distribution at thermospheric temperature. This excess of fast atoms also known as superthermal, suprathermal, or hot atoms, is indeed predicted by models [Shizgal and Linderfeld, 1980, Shematovich et al., 1994, Gérard et al., 1995]. Monte Carlo simulations of the hot oxygen geocorona by Shematovich et al. [1994] and Gérard et al. [1995] showed that the energy distribution function of the suprathermal oxygen population results from the non-linear interplay between the photochemical exothermal processes producing oxygen atoms, the thermalization of the produced fast atoms and transport through the thermosphere and exosphere. These theoretical results are supported by observation: Yee et al. [1980] deduced a density of 10^5 to 10^6 cm^{-3} hot O atoms at 550 km with a temperature of at least 4000 K, based on twilight measurements of $O^+(^2P)$ emissions at 732 - 733 nm. Likewise, Hedin [1989] inferred a concentration of hot $O(^3P)$ atoms up to ~10^6 cm^{-3} around 550 km under high solar activity conditions. This result relied on a comparison between satellite drag data and mass spectrometer measurements indicating a scale height anomaly which was attributed to the presence of a 3% population of superthermal $O(^3P)$ atoms at 4000 K.

Cotton et al. [1993b] used the Berkeley Extreme-ultraviolet Airglow Rocket Spectrometer (BEARS) on board a sounding rocket to measure the vertical brightness profiles of the oxygen emissions at 130.4 and 98.9 nm, showing an excess above 500 km compared to the expected theoretical profiles computed using a radiative transfer model. This anomaly was interpreted as a signature of the scattering of 130.4 and 98.9 nm photons by a population of hot oxygen atoms above the exobase. The hot oxygen population was modeled as having an ad hoc density profile, fitted to account for the observed intensity profiles, but lacking physical grounds, expressed as

$$n_h(z) = n_{h0} \exp\left\{-\frac{z - z_0}{H_h} - \sigma_{col}\left[n(z)H(z) - n(z_0)H(z_0)\right]\right\} \tag{1}$$

where n_{h0} is the hot O density at reference altitude z_0, $H_h = \frac{kT_h}{m_O g}$ is the hot O scale height at a temperature T_h (~ 4000 K) higher than the Maxwellian value, n(z) is the neutral density from the MSIS model [Hedin, 1991] with a scale height H(z). The elastic collision cross section σ_{col} was taken to be 3×10^{-15} cm^2, so that this expression implements a scale height approach based on a partial thermalization at the exobase. This population was added to the MSIS number density, resulting in increased scale height and concentration. The higher oxygen density then resulted in a larger line-wing scattering optical thickness of the exospheric medium at 130.4 and 98.9 nm, allowing an improved fit to the observations, despite the lack of physical grounds of the method.

Hubert et al. [1999] further analyzed the radiative transfer of the OI $2p^4\ ^3P$ — $2p^3\ 3s'\ ^3D^0$ 98.9 nm resonance multiplet, accounting for the presence of a non-thermal oxygen population, computed using the physics-based Monte Carlo model of Shematovich et al. [1994]. They used the resonance line radiative transfer model developed by Gladstone [1982, 1985] that uses the Feautrier method [Feautrier, 1964] with angle-averaged partial frequency redistribution (AAPR) and assumes a plane-parallel atmosphere. The primary photochemical excitation rate of the $2p^3\ 3s'\ ^3D^0$ was computed using the GLobal airglOW (GLOW) model [Solomon et al., 1988; Solomon and Abreu, 1989; Solomon, 2001; Solomon et al., 2001; Bailey et al., 2002]. The atmospheric composition was obtained from MSIS90 model [Hedin, 1991], which consists in a semi-empirical representation of the atmosphere that represents the diffusive equilibrium corrected to account for photochemical processes. The hot oxygen population was included as a fraction of the total oxygen density given by MSIS. With this more physical approach, Hubert et al. [1999] found that the inclusion of the hot oxygen population does indeed increase the modeled OI 98.9 nm intensity, but only up to a level insufficient to account for the BEARS sounding rocket measurement of Cotton et al. [1993a,b], obtained under high solar activity conditions ($F_{10.7}$= 173, $\overline{F}_{10.7} \simeq 156$ on September 30, 1988). None of these attempts to explain the observed OI 98.9 nm emission was thus satisfactory: the method used by Cotton et al. [1993b] to include a nonthermal population and account for the observation has no physical ground, and the detailed modelling of the suprathermal oxygen geocorona conducted by Hubert et al. [1999] failed to account for the observation. This research topic was then left unsolved and abandoned for several years and, as far as we know, no new research was attempted to explain the mystery until nowadays.

The FUV and EUV solar flux has been obtained at very high spectral resolution with the SOHO-SUMER instrument [Curdt et al., 2001], unexpectedly revealing a significant solar OI emission at 98.9 nm, i.e., a source of photons that had not been accounted for before in modeling the OI radiative transfer at that wavelength in the Earth thermosphere. Gérard et al. [2010] modeled the radiative transfer of the OI-98.9 nm emission in the thermosphere of Venus, including photochemical sources and resonance scattering of solar photons. Their results compared well with the Cassini UVIS EUV observation of the Venus thermosphere performed during the Cassini flyby of Venus, up to ~20% over the whole flyby with a much better accuracy over the portion of the flyby presenting the largest 98.9 nm intensity. These authorsshowed that, for this planet, resonance scattering of solar 98.9 nm photons is a major source of emission at high altitude.

In the present study, we model the radiative transfer of the OI 98.9 nm multiplet in the Earth thermosphere including resonance scattering of the solar photons that was not accounted for in previous studies. We also include the effect of the superthermal oxygen population. Theoretical results are compared with the intensity profiles measured with the BEARS sounding rocket and other, earlier observations from the STP78-1 satellite. We will also broaden the scope of our study to two other important oxygen emissions: the OI-130.4 and 135.6 nm multiplets, thus including the analysis of a second optically thick (at 130.4 nm) and an optically thin emission (at 135.6 nm).

2. Modeling

We use the Monte Carlo model described by Shematovich et al. [1994] to compute the non-thermal energy distribution function of thermospheric oxygen. Indeed, we use the same $O(^3P)$ energy distribution functions as those used by Hubert et al. [1999]. We did not use updated cross sections in order to ease comparison with previous studies. We do not expect updated cross sections would change the computed hot oxygen population by more than ~10%, which is the uncertainty of the Monte Carlo model results. The exothermal sources of fast oxygen atoms are thus those listed by Richards et al. [1994a] and Hickey et al. [1995]. The calculated non-thermal oxygen energy distribution function (EDF) depends on altitude, as does the hot oxygen abundance. **Figure 1** shows the oxygen EDFs at 500 and 600 km altitude, calculated under maximum solar activity conditions (F10.7 = 200). The superthermal oxygen population consists in the small disturbances found around ~1 eV, whereas the high energy hot tail at E > 2 eV, conspicuous in logarithmic scale, represents oxygen produced by one of the exothermal processes listed in **Table 1**, which have undergone only a few collisions and are thus still in the initial stages of the thermalization process. **Figure 2** shows the superthermal fraction $[O]_{hot}/[O]_{tot}$, the ratio of the hot oxygen to the total $O(^3P)$ densities calculated under solar minimum and solar maximum conditions (the hot oxygen population is just a small contribution in these results). Below the exobase (located around 600 km under maximum solar activity conditions), the ratio varies roughly linearly with altitude, until it starts increasing rapidly above the exobase. The non-thermal EDFs of **Figure 1** were obtained assuming that the total oxygen density profile is that given by the MSIS-90 model, which does not account for the increased scale height due to the hot oxygen population. Such an increase of the scale height implies that the total oxygen concentration should be higher than the MSIS density profile at exospheric temperature. We thus model the radiative transfer of the oxygen UV emissions under four different assumptions:

1. The oxygen density and temperature profiles are those of the MSIS model.
2. The total density remains unchanged, but has two contributions: one thermal at T_{MSIS} and one non-thermal at 4000 K, after Hedin and following the MC computation. The superthermal fraction will be that of the Monte Carlo simulation. This assumption implies an increase of the scattering optical thickness in the wings of the oxygen lines, producing an increase of the computed intensity.
3. Same as 2, but including a diffusive correction of the total density to account for the scale height modification due to the hot population, causing an increase of the scatterer density (as was already done by Hubert et al. [1999]).

4. The superthermal and thermal populations coexist, with separate diffusive equilibrium above the exobase, with the hot fraction given by the MC computation. The hot O population is assumed to vary linearly below the exobase, smoothly merging near the exobase. This assumption implies an increase of the scatterer density larger than that of hypothesis 3, as we will show in the next paragraphs.

Assuming that the thermal and non-thermal populations are separately distributed at diffusive equilibrium does not make sense below the exobase, where collisions thermalize the fast oxygen atoms and efficiently couple the hot and thermal oxygen populations. However, we consider this assumption as a rough, first order, correction above the exobase where collisions do not allow an efficient loss of the hot O energy to the thermal population. In order to include the hot oxygen population in the radiative transfer model under assumption 4, we fitted the ratio $\beta = [O]_{hot}/[O]_{MSIS}$ using the following expression:

$$\beta = \left(a + b\frac{r - r_0}{H_0}\right)W(r) + \beta_0\, exp\left(-\frac{m\, g_g R^2}{k\, T_0}\ \frac{T_0 - T_h}{T_h}\ \left(\frac{1}{r_0} - \frac{1}{r}\right)\right)\left(1 - W(r)\right) \tag{2}$$

where $W(r) = 1 - 0.5\left(1 + erf\left(\frac{r - r_0 - H_0\, w_{shift}}{\sqrt{2}\, H_0\, w_{sig}}\right)\right)$,

r is the geocentric distance, R is the planet radius, g_g is the gravity acceleration at the ground, k is the Boltzmann constant, m is the mass of the oxygen atom, r_0, T_0, and H_0 are the radius, temperature and scale height at the exobase respectively. The location of the exobase is determined such that the local scale height equals the collision mean free path with a cross section of 3 x 10^{-15} cm^2, i.e., the cross section value used by Cotton et al. [1993b] for their scale height approach density correction. The first term represents a linear contribution to β, introduced to describe the roughly linear part of the profile (shown in **Figure 2)** below the exobase. The exponential term in the expression for β is obtained by taking the ratio of two isothermal diffusive profiles (accounting for the dependence of g versus r) at different temperatures and densities. Parameters $w_{shift} = 0$; $w_{sig} = 0.5$ determine the location and width of the connection between the linear and exponential regimes, with the weighting function W(r) of equation (2) introduced to allow for a smooth transition between the collisional and exospheric regimes. The values of w_{shift} and w_{sig} were chosen to locate the transition at the exobase, across a characteristic length equal to the scale height: apparently a reasonable choice, though somewhat arbitrary. Parameters a, b, β_0 and T_h are fitting parameters determined to match, and extrapolate if necessary, the computed ratios of **Figure 2**, normalizing the total density to the MSIS density in that plot (which is equivalent to assuming that the hot fraction is a small part of the total density in the Monte Carlo computation). **Figure 3** shows the superthermal fraction β fitted to the Monte Carlo simulation results under maximum solar activity. The fitted value of T_h is ~ 10,500 K, which corresponds to 3/2 k T_h ~ 1.36 eV, typical of the exothermal processes producing superthermal $O(^3P)$ atoms. Similar results were obtained for the low solar activity simulation, so that the fitting parameters can be interpolated between both extremes for application at intermediate solar activity. **Table 2** lists the fitting parameters obtained under both solar minimum and maximum conditions. **Figure 4** shows the oxygen density profiles obtained from the MSIS-90 model and under hypothesis 3 and 4 described above, for high solar activity conditions. The largest total density is obtained assuming that the thermal and non-thermal oxygen populations are separately distributed at diffusive equilibrium according to their own temperature and scale height, especially at high altitude, far up in the exosphere.

We model the radiative transfer of the oxygen UV emissions at 98.9 and 130.4 nm using the radiative transfer code developed by Gladstone [1982, 1985], and already used by Cotton et al. [1993b] and Hubert et al. [1999], including the presence of a superthermal oxygen population. The nonthermal population is accounted for as a second scatterer having a high temperature in addition to the thermal oxygen population. The wavelength-dependent optical thickness is then computed accounting for both populations, and the radiative transfer is solved using the Feautrier method. The population of the sublevels of the ground state $O(^3P)$ atoms is nevertheless assumed to be at local thermodynamic equilibrium, while it is assumed that the photochemical reactions populate the sublevels of the upper states according to their degeneracy as their energies are nearly equal, an assumption already made by Link et al. [1988]. The primary source of UV photons at 98.9, 130.4 and 135.6 nm is mainly twofold: photochemical sources (i.e., photoelectron impact excitation of O atoms) and resonance scattering of photons of solar origin. The 130.4 nm multiplet is also populated by branching from the upper state of the OI 102.7 nm multiplet. The 135.6 nm ^3P – $^5S^o$ transition is dipolar forbidden and only excited by photoelectron impact (this includes the cascade from the 3p ^3P level at 777.4 nm). The photochemical sources are calculated using the latest version of the GLOW model [Solomon, 1988] (freely available under Open Source Academic Research License Agreement) adapted to account for the modified oxygen density profile when needed.

The GLOW model uses a Crank-Nicholson method to compute the transport of photoelectrons through the Earth thermosphere with a two-stream assumption. In this model, the EUV solar flux is obtained from the EUVAC model between 50 and 1050 Å [Richards et al., 1994b]. Between 18 and 50 Å, the Hinteregger spectrum [Hinteregger et al., 1981] is scaled using the EUVAC algorithm. Below 18 Å, several sources are aggregated to estimate the solar flux, e.g. De Jager [1964], Smith and Gottlieb [1974], Manson [1977], Kreplin et al. [1977], Horan and Kreplin [1981], and Wagner [1988]. The FUV flux is scaled from the Woods and Rottman [2002] spectrum. The photochemical sources of excited oxygen are mainly electron impact on oxygen atoms and dissociative recombination of O_2^+. The interested reader is referred to the list of reactions available with the GLOW source code which is freely available and to the literature [Nagy and Banks, 1970; Solomon et al., 1988; Solomon and Abreu, 1989; Solomon, 2001; Solomon et al., 2001; Bailey et al., 2002].

In addition to the sources computed by the GLOW model, radiative recombination of O^+ producing the $^5S^0$ state is accounted for [Tinsley and Christensen, 1973]. The contribution of this mechanism can be considered negligible for the 3s $^3S^0$ state, i.e. for the 130.4 nm excitation. Our modelling of the OI 98.9 nm emission also includes production of oxygen in the 3s' $^3D^0$ state (via the 3p ^3F state) by dielectronic recombination [Abreu et al., 1984]. We use the reaction coefficient of Bates [1962] and the needed ionospheric properties come from the IRI model [Bilitza, 1990] used by GLOW. The O^+ concentration relevant for the conditions of the BEARS sounding rocket launch is shown in **Figure 4**. The 3s $^3S^0$ upper state of the OI - 130.4 nm transition is also populated by the 1127.8 nm transition from the 3d $^3D^0$ state to the 3p ^3P state followed by the transition at 844.6 nm to the 3s $^3S^0$ state. Transition between the 3d $^3D^0$ state and the $2p^4$ ^3P ground state occurs at ~102.7 nm forming a sextuplet of FUV lines with large Einstein transition parameters, so that optically thick radiative transfer of the OI 102.7 nm multiplet is also modelled to assess the sources of the OI 130.4 nm emission. The photochemical sources of the 3d $^3D^0$ state come again from the GLOW model.

The solar fluxes at 98.9, 102.7 and 130.4 nm are estimated using the proxy model of Woods and Rottman [2002] to derive values consistent with the $F_{10.7}$ activity index, as was already successfully done by Gérard et al. [2008, 2010] and Hubert et al. [2010] to model the radiative transfer of the optically thick oxygen UV multiplets at 98.9 and 130.4 nm through the atmosphere of Venus and compare the model results with the Cassini-UVIS observations. The proxy model derived by Woods and Rottman [2002] has a spectral resolution of 0.5 nm, too crude to resolve the spectral contributions at 98.9 nm. Using the high spectral resolution model of Tobiska [2004] it was determined that the OI 98.9-nm multiplet contributes ~24 %

to the total in the interval ranging from 98.5 to 100.5 nm under high solar activity conditions. For comparison, the OI 98.9 nm contribution to the quiet Sun high resolution spectrum of Curdt et al. [2001], measured using SOHO-SUMER, in that same interval is estimated to be ~19%. The contribution of the solar OI - 102.7 nm emission between 100.5 and 106.5 nm is estimated to be ~4.2% from the spectrum of Curdt et al. [2001] while the Lyman-β line contributes ~42%. Because the OI 130.4 nm solar emission is very intense, it is not necessary to make a similar correction to the flux deduced from the proxy of Woods and Rottman [2002] for this emission feature. The shape of the OI 130.4 nm multiplet solar line is derived according to the analysis of Gladstone [1992], who fitted the observed solar OI-130.4 nm multiplet line shapes from the Solar Maximum Mission (SMM) satellite using two offset Gaussian functions. The offset and FWHM of the Gaussian functions were separately estimated for each line of the multiplet. The line shapes of the solar OI-98.9 and 102.7 nm multiplets are poorly known. Average values of the parameters obtained by Gladstone [1992] for the 130.4 nm lines were used for these multiplets, as was already done by Gérard et al. [2010] for the OI 98.9 nm emission. The OI 102.7 nm system of lines has an additional source, known as the Bowen mechanism [Bowen, 1935], due to an incidental resonance with the broad solar HI-Lyman- β line at 102.6 nm. We compute the wavelength-dependent optical thickness of oxygen and its absorption of the solar HI Lyman-β, which provides an additional source of excitation of the 102.7 nm upper states and enters the radiative transfer process. The Lyman-β contribution to the solar flux is estimated to be ~42% between 100.5 and 106.5 nm based on the SOHO-Sumer spectrum of Curdt et al. [2002], and the Woods and Rotman [2002] proxy is used again to estimate its value. We account for the solar Lyman beta line shape assuming it is the sum of two offset Gaussian functions having the offset and FWHM values determined by Gladstone [1988]. The optically thick source function of radiative transfer is used to compute the production rate of the 3s $^3S^0$ state by branching from the 3d

$^3D^0$ state. The branching ratio is ~30% according to the Einstein transition parameters of Wiese et al. [1996]. For the conditions of September 30, 1988, the O I 98.9, 102.7 and 130.4 nm solar fluxes are found to be 6.74 x 10^8, 5.9 x 10^8 and 1.26 x 10^{10} photons cm^{-2} s^{-1} respectively while the H I Lyman-β flux is 6.00 x 10^9 photons cm^{-2} s^{-1}..

In our simulations, the primary excitation rate due to photochemical sources are distributed between the sublevels of the upper state proportionally to their degeneracy. This assumption considers that the population of sublevel k is propotional to g_k x exp(-E_k/kT) with all the E_k's being nearly equal. In the absence of data detailing the distribution of the 98.9 nm solar intensity between the members of the multiplet, it is assumed that the total flux is distributed among the singlet, doublet and triplet of lines in which the sextuplet is decomposed (see next paragraph) according to the degeneracy of their upper level, while, inside of the sub-multiplets (namely the doublet and the triplet), the flux is equally shared between the different lines that compose it.

The OI 98.9 nm multiplet results from the transitions between the oxygen $2p^4$ ^3P ground state and the excited $2p^3$ 3s' $^3D^0$ state. Applying the selection rules of spectroscopy, this transition system is a sextuplet of lines, decomposed into three sub-multiplets according to their upper sub-level (Table 3): a singlet (the transition at 98.8773 nm originating from the 3s $^3D^0_{J=3}$ level), a doublet (the transitions at 98.8655 and 99.0204 nm originating from the 3s $^3D^0_{J=2}$ level) and a triplet of lines (the transitions at 98.8578, 99.0127 and 99.0801 nm originating from the 3s $^3D^0_{J=1}$ level), without mixing between the components [Meier, 1991, Link et al. 1988], i.e. the wavelength separation between the lines of the multiplet is so large compared with the Doppler width at local temperature that a photon emitted in a transition can only be reabsorbed (and scattered) by the same transition, thus avoiding radiative coupling between the sub-multiplets.

Excited atoms in the $^3D^0$ state do not only relax directly to the ground state, but can also decay through intermediate energy levels, leading to (among others) the transitions at 799 and 117.2 nm. These branching transitions result in a loss of population through transition branching, that removes photons from the 98.9 nm radiation field during the radiative transfer process. This effect is accounted for in the radiative transfer modeling using a single scattering albedo (ω_0) amounting to 0.99972, 0.9975 and 0.99953 for the singlet ($O(^3P_3) \leftarrow O(3s'\ ^3D_3)$), doublet ($O(^3P_{2,3}) \leftarrow O(3s'\ ^3D_2)$) and triplet ($O(^3P_{1,2,3}) \leftarrow O(3s'^3D_1)$) of lines respectively, that we deduce from the Einstein transition parameters of the 98.9, 799 and 117.2 nm emissions provided by Wiese et al. [1996]. The OI-130.4 nm multiplet results from transitions between the OI $2p^4\ ^3P$ and $3p\ ^3S^0$ states. It is a triplet of lines coupled with a common upper state. The transition parameters that we use in modeling the 130.4 nm radiative transfer are taken from Wiese [1996]. The oxygen energy levels are from Moore [1993]. We neglect branching from the $3p\ ^3S^0$ state through the transitions at 164.13 nm (to the $2s^22p^4\ ^1D$ state) and at 232.5 nm (to the $2s^22p^4\ ^1S$ state) as their Einstein transition parameters are rather low, 1.83×10^3 and 4.61 s^{-1} respectively, resulting in a single scattering albedo of 0.999997 sufficiently close to 1 to be ignored.

For the $2p^4\ ^3P$ - $3d\ ^3D^0$ transition producing the OI 102.7 nm emission and radiative transfer, we follow the approximation previously made by Meier [1991] and by Cotton et al. [1993]. The sextuplet is separated into a triplet ($O(^3P_{1,2,3}) \leftarrow O(3d\ ^3D_1)$), a doublet ($O(^3P_{2,3}) \leftarrow O(3d\ ^3D_2)$) and a singlet ($O(^3P_3) \leftarrow O(3d\ ^3D_3)$) of lines (Table 3) assuming they can be treated separately. However the small wavelength separation between the lines of the multiplet allows for a partial coupling across the whole sextuplet. The uncoupling approximation has nevertheless proven valid because of the large branching towards the $3p\ ^3P$ state via the 1127.8 nm transition, and because ~85% of the 102.7 nm radiation field is expected to be found in the singlet [Meier, 1991 ; Meier et al. 1987].

3. Simulation results.

The vertical profile of the $2p^3\,3s'\,{}^3D^0$ primary source of photons calculated for the conditions of the BEARS sounding rocket launch of Cotton et al. [1993a,b] using the MSIS-90 oxygen concentration profile is shown in **Figure 5** while **Figure 6** shows the upward and downward photoelectron fluxes computed with the GLOW model without hot oxygen correction. The effect of the hot oxygen corrections considered in this study were estimated and found to remain lower than 4% at worst at all altitudes. The photoelectron fluxes peak at roughly the same altitude as the primary source function, which highlights that the photochemical sources computed by the GLOW model are dominated by photoelectron-impact processes in the lower thermosphere. The primary source (**Figure 5**) represents the rate at which new 98.9 nm photons are introduced into the radiative transfer process by photochemical processes (computed with the GLOW model) and by resonance scattering of solar 98.9 nm photons. It should not be confused with the source function of radiative transfer which represents the number of excited atoms emitting a 98.9 nm photon per second in a unit volume, including the effects of multiple scattering. The contribution of the photochemical sources calculated using the GLOW model (mainly electron impact on oxygen atoms) dominates that of resonance scattering of the solar flux at 98.9 nm at low altitude, while at high altitude, above ~450 km, the resonance scattering primary source dominates over the photochemical processes. The primary source integrated across the whole vertical profile nevertheless remains dominated by the photochemical processes. Inclusion of the hot oxygen population results in an increase of the primary source at high altitude, with a larger increase found when the hot and thermal oxygen populations are assumed to be separately distributed at diffusive equilibrium. This naturally stems from the larger density found in that case above the exobase. The total radiative transfer source function of the OI 98.9 nm multiplet is detailed in **Figure 7**. The radiative transfer is computed separately for the photochemical and resonance scattering primary sources, and summed up afterwards. Indeed, the ground state oxygen concentration is not significantly modified by the transfer of the FUV radiation in the thermosphere so that both sources do not need to be combined to compute the radiative transfer. The altitude-dependent relative importance of the photochemical and solar primary source of photons discussed above also appears in the radiative transfer source function: the solar source becomes important at high altitude only, but the photochemical source remains dominant up to a larger altitude (~675 km) because of the very large photon primary production at low altitude. Inclusion of the hot oxygen population without modifying the total density only increases the optical thickness in the wings of the line shape. It does not make a large difference compared with the MSIS90 reference run, as already pointed out by Hubert et al. [1999]. Inclusion of the density corrections proposed above in the second paragraph (assumptions 3 and 4) produces an increase of the optical thickness of the atmosphere proportional to the density enhancement. This results in a more efficient entrapment of the 98.9 nm photons in the thermosphere that causes an increase of the radiative transfer source function.

The source function is not directly observable. The BEARS 98.9 nm intensity profile measured by Cotton et al. [1993b] is shown in **Figure 8**, along with the modeled intensity. The MSIS90 thermal population suffices to account for the observation at low altitude.It could also be considered acceptable above the exobase, owing to the uncertainties affecting the observation. This is a major difference with the simulations of Cotton et al. [1993b] and Hubert et al. [1999] who could not account for the observation in a satisfactory manner because their simulation lacked the inclusion of the resonance scattering of the solar 98.9 nm multiplet. Consideration of the superthermal population without modifying the total density slightly increases the modeled intensity. The diffusive correction accounting for the higher temperature due to the hot oxygen component makes a more significant correction, and the modeled intensity does apparently better match the observation, considering both data points at 600 and 750 km. Inclusion of the separate diffusive equilibrium produces a modelled intensity profile that passes over the observed one, whether the calculated solar maximum superthermal population is used or whether an interpolation (versus the F10.7 index) between the solar minimum and maximum profiles is used (solar activity was already high at the time of the BEARS sounding rocket launch). In the present case, inclusion of the superthermal population with its own diffusive equilibrium appears as an upper bound to the total oxygen density considering the EUV intensity measurement. The new key parameter to consider in order to account for the observed 98.9 nm intensity at high altitude is clearly scattering of the solar multiplet.

The simulated intensity for a downward looking geometry from a distant vantage point (i.e. the emerging intensity) can be compared with the intensity obtained for the same line of sight geometry assuming optically thin conditions and neglecting O_2 absorption. Neglecting the effect of the suprathermal atoms, these two intensities are 1.116 and 0.921 kR. In first view, one would expect the optically thick intensity to be larger than the optically thin result, because multiple scattering breaks the isotropic distribution of the primary emission and favors the upward direction by essentially reflecting upwards the downward-propagating photons, as already underlined by Link et al. [1988] concerning the 130.4 nm radiation. The opposite is found because of the absorption by O_2 and, mainly, because of the non-unit single scattering albedo of the 98.9 nm multiplet which causes a “leak” of 98.9 nm photons during the radiation transfer through the thermosphere. The radiative transfer of the photons of solar origin contributes ~0.211 kR to the emergent intensity, i.e. ~19% of the total. Under the optically thin assumption, it is ~0.0970 kR, i.e. ~11% of the total. Because the primary source function associated with the resonance scattering of the solar 98.9 nm multiplet peaks at a higher altitude, it is not absorbed by O_2. The optical depth of the emitting layer being lower than that of the photochemical source, the single scattering albedo leakage is also less important. We then retrieve the intuitively natural trend: the computed optically thick intensity is larger than the optically thin one. These numbers also highlight that resonance scattering of the solar 98.9 nm photons does not dominate the column-integrated source function, and is only important at high altitude. Including the hot oxygen correction does nearly not modify the calculated emergent intensities. Indeed, the hot-O correction is important at high altitude where the gas density is lower, far from the peak of the photoelectron fluxes, so that the photochemical sources computed by the GLOW model are only weakly modified by this correction. Moreover, including the suprathermal oxygen correction results in an increase of the optical thickness of the high altitude layers, where the solar radiation is resonantly scattered. But the solar flux itself is not modified, so that the radiative energy input from the solar 98.9 nm multiplet remains nearly unchanged. This explains why the contribution of the resonance scattering of the solar 98.9 nm radiation to the emergent intensity is nearly not sensitive to the presence of the hot oxygen population as well.

Figure 9 shows the primary source, the source function and the intensity computed for the OI 130.4 nm triplet. As it is well known, the scattering of the solar 130.4 nm flux, which amounts to 1.14 x 10^{10} ph cm^{-2} s^{-1} in our simulation according to the proxy of Woods and Rotman [2002] (about twice as large as the value reported by Cotton et al. [1993a]), largely dominates the primary source and the source function at high altitude. We inferred, based on the solar spectrum of Curdt et al. [2001], that the 130.22, 130.49 and 130.60 nm lines of the multiplet contribute 32%, 33% and 35% to the total intensity of the solar triplet, respectively, i.e. about one third of the photons in each member of the triplet. This result is similar to that obtained from the high resolution semi-empirical spectrum of Killen et al. [2009] which gives 36%, 33% and 31% respectively. The computed intensity, for a 97° zenith angle look direction, is shown in the third panel with the BEARS measurement. The conclusions are similar to those obtained at 98.9 nm. The intensity simulated using the MSIS90 atmosphere accounts fairly well for the data, although the simulation including the hot oxygen atoms and a modified diffusive equilibrium seems to somewhat better account for the observation at high altitude. Assuming the thermal and nonthermal oxygen populations are at separate diffusive equilibrium obviously produces an overestimate of the intensity at high altitude, and should be considered as a lower bound. At low altitude, the calculation slightly underestimates the 130.4 nm intensity up to ~500 km, i.e. the altitude where the resonance scattering of the solar multiplet starts to dominate the optically thick source function. This discrepancy can likely be attributed to a slight underestimate of the photochemical source of excitation of the 3s ^{5}S state by the GLOW model. Figure 10 recapitulates the intensity profiles simulated at 98.9 nm and 130.4 nm using the MSIS atmosphere, corresponding to the conditions prevailing for the BEARS sounding rocket launch. We also show the 135.6 nm and the 1027 intensity profiles. Scattering of the solar light is totally negligible for the 135.6 nm multiplet, while it is important for the other emissions, especially at high altitude.

We now compare our model with FUV and EUV measurements of the OI emissions at 98.9, 130.4 and 135.6 nm obtained with the EUV spectrometer onboard the USAF STP78-1 satellite [Bowyer et al., 1981; Chakrabarti et al., 1983]. We simulate the radiative transfer of the OI 98.9 and 130.4 nm emissions for the conditions prevailing at the time of each individual STP-78 observation, which consist in EUV and FUV spectra recorded during a rotation of the spinning satellite, thus producing angular scans. The background is interpolated from the neighboring wavelength bins of each spectral feature and subtracted. The superthermal oxygen population is obtained by interpolating the hot oxygen fraction versus the F10.7 index between the Monte Carlo simulation results obtained under solar minimum and solar maximum conditions. **Figure 11** shows the 98.9 nm intensity measured during two STP78 orbits on 21 March 1979, i.e., at the equinox (F10.7 = 181). On that day, we estimate using the Woods and Rotman [2002] proxy that the solar fluxes of the OI 98.9, 102.7 130.4 nm multiplet and of the H I Lymanβ line are ~6.98 x 10^8, ~6.20 x 10^8, ~1.28 x 10^{10} and ~6.30 x 10^9 photons cm^{-2} s^{-1} respectively. The data were selected in a latitude interval between -20° and -30°, with the longitude ranging between 160° and 170°. The solar zenith angle ranged between 20° and 30°. The STP78 orbit was nearly circular at 600-km altitude. Although the satellite altitude did not vary significantly during one orbit, we nevertheless account for its exact value in simulating the observation using the radiative transfer model. The data shown in **Figure 11** were accumulated during 10 rotations of the satellite and averaged into viewing zenith angle bins. **Figure 11** also shows the calculated intensity, separating the contributions of the photochemical primary source and the resonant solar source at 98.9 nm. Inclusion of the superthermal $O(^3P)$ population to the MSIS90 oxygen density profile causes an increase of the modeled intensity for upward looking directions. The overall shape of the modeled angular scan reproduces the observed one fairly well, but the agreement is not as good as was found for the BEARS sounding rocket measurements. However, it must be noted that the solar flux used in our modeling is uncertain, so that a strict quantitative agreement is not really expected. Moreover, the uncertainty on absolute calibration of the spectrometer onboard STP78-1 was estimated by Link et al. [1988] to be ~20% at 98.9 nm.

Figure 12 shows the brightness of the OI 130.4 and 135.6 nm multiplet observed by STP78 and modeled using the MSIS90 atmosphere (dotted lines), including the non-thermal oxygen correction (solid lines) under conditions identical to those of **Figure 11**. The 135.6 nm emission rate is calculated using the GLOW model [Solomon et al., 1988] and integrated along the lines of sight passing by the STP78-1 location for viewing zenith angles ranging from zenith (0°) to nadir (180°) direction. The computed 130.4 nm intensity is overestimated by roughly a factor 2. Multiplying the total intensity computed accounting for the hot oxygen population and applying diffusive equilibrium by a factor ~0.6 produces a good fit to the data. The intensity computed using the MSIS90 density also agrees fairly well with the observed angular scan at the expense of a similar correction factor, considering the uncertainties of the measurements and those of the model. It must be noted that Link et al. [1988] estimated the accuracy of the STP78 absolute calibration to ~50% at 130.4 and 135.6 nm, so that the discrepancy between the modelled and observed 130.4 nm intensity remains acceptable, given that the shape of the computed angular scan fairly corresponds to the observed one. The computed 135.6 nm profiles were smoothed to account for the effective field of view of the spectrometer, resulting from a complex combination of the actual field of view of the instrument and the satellite motion. The shape of the modeled, optically thin OI 135.6 nm brightness angular scan differs somewhat from the observed profile while the absolute value at the peak brightness is fairly well modeled within a factor ~2. Differences in shape can be due to a too small background removal which is performed by interpolating the spectrum from the neighboring wavelength bins, as can be guessed from the residual intensity for upward looking directions or, more likely, to the complicate triangular effective field of view of the observation, that combines the instrument aperture (the STP78-1 instrument slit was large indeed) and the spinning motion of the spacecraft. This issue is without doubt a source of uncertainty at all wavelengths. We verified on more than 100 angular scans that, for upward looking directions, the signal to noise ratio (computed after background subtraction) is very poor at 135.6 nm, generally around 1, making the results very sensitive to an underestimate of the subtracted background. Indeed, one would expect the 135.6 nm signal to decrease to 0 as the observing zenith angle decreases. Consequently, we do not trust the 135.6 nm data obtained under upward looking direction. Inclusion of the superthermal oxygen population with the consistent diffusive equilibrium correction does not make a substantial difference.

Figure 13 shows the OI 98.9, 130.4 and 135.6 nm multiplet intensities averaged over two STP78-1 full orbits, on 21 March 1979. Only daytime data are selected, excluding the terminator and south Atlantic anomaly regions. The detailed modelling of each emission is computed for each of the 130 STP78-1 angular scans that were found and selected, and the averaged intensities are then computed so that they can be compared with the observation. A scaling factor is applied to the computed total intensities to fit the data in a least squares sense, in order to cope with the uncertain solar flux. We find, once again, that scattering of solar photons makes a significant contribution to the 98.9 nm radiative transfer at high altitude, amounting to nearly 25% for a horizontal viewing geometry at ~600 km. The general trends described above based on **Figures 10 and 11** appear again in the 2-orbits average: inclusion of the superthermal oxygen population with adapted diffusive equilibrium allows for a slightly better agreement with the observed OI-98.9 nm angular scan. Resonance scattering of the solar 98.9 nm multiplet makes a significant contribution for upward-looking directions, producing a modelled intensity profile that better corresponds to the observed one. Similar conclusions are reached concerning the OI-130.4 nm intensity. The observed detailed shape of the peak of the 135.6 nm emission is reasonably well reproduced by the theoretical simulations, but the smoothing that we apply to account for the effective aperture of the instrument may not be sufficient for the optically thin 135.6 nm emission. Inclusion of the nonthermal atoms in the simulation makes no significant difference. Again, we do not trust 135.6 nm data obtained for upward looking directions.

4. Discussion.

We have revisited the radiative transfer of two important atomic oxygen multiplets in the Earth's thermosphere and exosphere. This analysis was motivated by the relatively recent observation of the OI-98.9 nm multiplet in high resolution solar spectra, i.e., a source of photons that had not been accounted for in past studies of that multiplet, in an attempt to explain the previously reported anomaly in the 98.9 nm intensity observed above the exobase. We used the MSIS90 atmosphere model to describe the thermospheric and exospheric gas and included the previously-modelled effects of a superthermal oxygen geocorona using several approximations. First, splitting the total MSIS90 $O(^3P)$ density into a thermal and a non-thermal fraction barely influences the modelled radiative transfer of the oxygen multiplets (as previously reported by Hubert et al. [1999]), despite the increase produced in the optical thickness in the wings of the optically thick spectral line shape. Correcting the MSIS90 density profile for the larger oxygen scale height (resulting from the presence of the hot oxygen population), produces a total density increase sufficient to account for the BEARS sounding rocket measurement at 98.9 nm above the exobase. Applying a more radical correction by adding a hot oxygen population in diffusive equilibrium (i.e., having its own scale height) produced an increase in the modelled 98.9 nm intensity above the exobase that exceeds the BEARS-observed profile, and thus appears as an upper bound correction. Indeed, up to our knowledge, no previous study inferred an oxygen density as large as what we calculate under that assumption (except for Cotton et al. [1993b]). We find that scattering of solar photons produces a significant contribution to the 98.9 nm radiative transfer at high altitude, above ~450 km and in the exosphere, that is necessary to account for the observation with only moderate modification of the MSIS90 density profile. Simulations of the OI-130.4 nm multiplet show that the hot oxygen correction that we apply is compatible with the observed BEARS intensity profile at 130.4 nm. Our simulations also fairly reproduce the intensity observed by the STP78-1 satellite at 98.9, 130.4 and 135.6 nm. Inclusion of the solar 98.9 multiplet in the model produces a better agreement with the observation. Including the hot oxygen population also improves the agreement with the data for upward looking directions, but the associated intensity increase remains comparable with the error affecting the data. The modelled 135.6 nm intensity is in fair agreement with the STP78-1 observed intensity given the uncertainties on the absolute calibration and the complicate effect of the instrumental effective aperture. Inclusion of the nonthermal oxygen atoms makes no substantial difference. As already pointed out by Link et al. [1988], the 135.6 nm can be contaminated by a contribution from the N_2 Lyman-Birge-Hopfield band. We simulated the LBH intensity using the GLOW model and the spectrum measured by Ajello and Shemansky [1985], and found it can contribute ~30% to the 135.6 nm channel, as was already estimated by Link et al. [1988]. This contamination nevertheless remains below the uncertainty on the absolute calibration, and it was not included in the figures presented here.

We also simulated the 98.9, 130.4 and 135.6 nm intensities using the Atmospheric Ultraviolet Radiance Integrated Code (AURIC) model [Strickland et al., 1995, 1997, 1999, Swaminathan et al., 1998, Siskind et al., 1995, Majeed et al., 1997]. This model has a more sophisticated solver that uses a multistream approximation, while the GLOW model uses a 2-streams Crank-Nicholson method. We refer the interested reader to the literature and to the documentation freely available from Computational Physics INC. for a detailed description of the AURIC model. Although the intensities computed with the AURIC model slightly differ from those of the GLOW model, the main results discussed above remain: scattering of the solar 98.9 nm multiplet is an essential contribution to the 98.9 nm radiative transfer at high altitude, inclusion of the suprathermal oxygen population produces a slight increase of the OI 98.9 and 130.4 nm intensity in the exosphere, while it makes no significant difference at 135.6 nm. It must also be kept in mind that the uncertainties on the solar flux (both the ionizing EUV radiation and the 98.9 and 130.4 nm incident fluxes) are such that applying a correction factor (not too different from 1) to the computed intensity is generally an acceptable fix that reconciles the model and the observation, providing that the overall shape of the modelled profiles sufficiently resemble the observation (which was not the case at 98.9 nm before inclusion of the solar source).

Because scattering of 98.9 nm solar radiation is the major contribution to the primary source of photons at exospheric altitudes, a detailed knowledge of the spectral distribution of the multiplet lines would be needed for successful modelling. Indeed, we used a rough approximation assuming that the solar 98.9 nm line shape could be deduced from the optically thick 130.4 nm solar line shape, fitted using two offset Gaussians. Because the transition parameters of these two multiplets are different, it is not obvious that this assumption is sufficiently accurate. Only a detailed measurement of the solar 98.9 nm line shape at very high spectral resolution could lead to a reliable improvement in our knowledge of the solar 98.9 nm optically thick spectral distribution. It can be expected that a narrower spectral distribution of the solar radiation would allow for more incident photons to be scattered by oxygen atoms before being absorbed by O_2 molecules deeper in the atmosphere, thus increasing the number of photons undergoing radiative transfer at high altitude, and perhaps producing a larger computed intensity above the exobase. This would reduce the need for an increased exospheric oxygen density. Estimating the quantitative magnitude of this effect will, however, remain beyond reach until the detailed solar line shapes of the 98.9 nm multiplet are known. Moreover, the absolute value of the 98.9 nm solar flux is itself an important source of uncertainties. The whole modelling is indeed sensitive to the solar flux: the photochemical production rates are proportional to the solar flux, and also depends on its spectral shape. The resonance scattering primary sources at 98.9 and 130.4 nm do also depend on both the absolute flux, but also on its distribution among the members of the multiplet and on the detailed high resolution line shape of the solar lines, which is unknown except for the 130.4 nm multiplet. Despite these uncertainties, agreement with the BEARS data is satisfactory, without the need of any scaling of the modelled intensity. The agreement is not so good with the STP78 data, but the uncertainties on the absolute calibration of that spectrometer are also large, so that one can consider applying a multiplication factor to better model the data. The shape of the modelled intensity angular scans is then fairly well reproduced by the modelling.

We also attempted to use the interesting semi-empirical spectrum of Killen et al. [2009] in the EUV. Fitting a Gaussian function to lines of the OI-989 multiplet, it appears these lines have an FWHM of ~0.041 Å, i.e. representative of a temperature of ~53000 K (a temperature that can easily be reached in the transition region between the solar chromosphere and the corona). Also, the total intensity is distributed between the triplet ($O(^3P_{1,2,3}) \leftarrow O(^3D_1)$), doublet ($O(^3P_{2,3}) \leftarrow O(^3D_2)$) and singlet ($O(^3P_3) \leftarrow O(^3D_3)$) proportionally to the degeneracy of the upper state (which, up to ~0.03%, is equivalent to a thermal population of the upper sub-levels) while inside of a given sub-multiplet, the intensity is distributed proportionally to the Einstein spontaneous transition parameters. The OI- 989 Å total intensity is however rather weak in that spectrum: it contributes to ~1.2% of the total between 985 and 1005 Å, in contrast with the observed SOHO-SUMER spectrum [Curdt et al., 2001] for which we find ~19% (27% if the continuous background is removed). The Gaussian shape does however concentrate proportionally more photons near the line center than the two-offset Gaussian shape used above. This does however not fully compensate for the much lower flux predicted by this spectrum. Using these spectral properties and applying the same procedure as above to estimate the total OI-989 solar intensity, we naturally find that the solar source provides a small contribution to the 989 radiation field at high altitude, so that is becomes difficult to account for the BEARS observation.

The suprathermal oxygen density correction that we apply here assumes that the hot oxygen population produces a temperature increase that modifies the oxygen scale height and diffusive profile above the exobase. In the absence of collision, this approximation could be insufficient far above the exobase. The assumption of separate diffusive equilibrium for the thermal and nonthermal oxygen population nevertheless produces an upper bound, and the real profile may be between these two approximations. The BEARS observed OI intensities at 98.9 and 130.4 nm are nevertheless compatible with the simple diffusive equilibrium assumption.

Our radiative transfer model assumes that the ground state oxygen atoms $O(^3P)$ are at local thermodynamic equilibrium (LTE), i.e. that the population of the $O(^3P)$ sublevels is proportional to the degeneracy of each level, given that the sublevels have nearly the same energy. In the thermosphere, this assumption is valid because collisions occur sufficiently often to maintain the LTE population. However, in the exosphere, collisions are less frequent and a departure from equilibrium can occur. Cotton [1991] analyzed the effect of non-LTE population of the $O(^3P)$ sublevels on the OI-130.4 nm radiative transfer, accounting for collisions, fine structure radiative decay and resonance scattering, iteratively running a radiative transfer code to consistently estimate the non-LTE population accounting for the three processes. He found that the collisional lifetime largely dominates below 600 km (i.e. about the exobase) but that radiative decay and resonance scattering begin playing a role above that altitude.

We developed a model of the non-LTE (NLTE) population of the ground state oxygen that uses the more recent reaction cross sections of Zygelman et al. [1994] describing the non-elastic collisions between oxygen atoms in the ^3P state. We also included the effect of electrons using the reaction rate coefficients of Péquignot [1990]. Infrared relaxation of the upper state of the multiplet is included using the Einstein transitions parameters $A_{J=1\rightarrow J=2}$= 8.9 x 10^{-5} s^{-1}, $A_{J=0\rightarrow J=2}$= 1.34 x 10^{-10} s^{-1} and $A_{J=0\rightarrow J=1}$= 1.75 x 10^{-5} s^{-1} [Froese Fisher and Saha, 1983]. Sharma et al. [1994]] did also use these reaction coefficients to study the NLTE population of ground state oxygen up to ~600 km and detail the equilibrium relations balancing the production and loss rates of the ground state sub-levels. They found that the ground state oxygen population very closely remains at LTE up to the exobase. We introduced the effect of collisions with molecular oxygen and nitrogen to enforce that the distribution will remain at LTE at very low altitude. In the absence of any knowledge of the needed cross sections, we estimated them roughly by summing the relevant cross sections from Zygelman et al. [1994] and apply a scaling by the mass of the colliding partner. This procedure does not pretend to provide accurate cross sections: it is only introduced as a rough first guess that will warranty LTE at low altitude (where it would in principle not be necessary as collisions between atomic oxygen atoms are very frequent and opposite processes satisfy the detail balance conditions). We also include the effect of UV radiative transfer on the NLTE distribution of the ground state sublevels using an iterative method. Absorption of radiation is computed for every modelled UV multiplet using the wavelength-dependent angle-averaged intensity as explained by Mihalas [1978], which contribute as loss rates for the ground state sub-levels. The radiative transfer source functions (again detailed for every line of every modelled multiplet) contribute to the production rate of the ground state sublevels (a small correction is applied to cope with the single scattering albedo, so that the total production and loss rates of the ground state sublevels, associated with the UV radiation field, are equal for obvious reasons of conservation of the total number of particles). To start the iterative resolution, we first solve for the NLTE distribution of the ground state oxygen neglecting any radiative transfer effect. The radiative transfer (of the 102.7, 130.4 and 98.9 nm multiplets) is solved using that NLTE result, and the output is used to retrieve the NLTE population including the radiative transfer results. The procedure is repeated iteratively using the newly-computed NLTE population until the maximum relative change of population across the whole vertical profile is found to be smaller than 0.2% from one iteration to the other. This threshold was chosen to limit the number of iterations, as the iteration process is compute-intensive, while still obtaining a sufficiently good estimate of the NLTE population.

Figure 14 shows the NLTE population that we obtain using this method, under the conditions prevailing for the BEARS sounding rocket launch. Clearly, The population nearly follows the LTE distribution up to ~600 km, i.e. near the exobase. At higher altitude, a surprising result is found: the J=0 level is more populated than under LTE conditions. We found that this is due to 2 processes: first, the electron collision reaction rates of Péquignot [1990] favor the excitation of the J=0 level. Second, the radiative transfer modifies the NLTE population of the $O(^3P)$ sublevels. Indeed, we verified that accounting for the inelastic collisions between $O(^3P)$ atoms only (and the infrared relaxation), the population would tend to concentrate in the J=2 sublevel as the altitude is increased. This result was obtained using the MSIS atmosphere. Accounting for the non-thermal distribution of the kinetic energy of the oxygen atoms slightly modifies the picture, especially above ~1000 km, but not as to dramatically change the total intensity of the UV multiplets resulting of radiative transfer in the altitude range where the BEARS data were obtained.

The effect of the NLTE population on the modeled 98.9 nm intensity is shown in **figure 15**. The computed total intensity is very nearly the same as the LTE result shown in **figure 8**, although, as pointed out by Cotton et al. [1991], the detailed relative importance of the lines of the multiplet can be modified. It remains that scattering of the solar 98.9 nm multiplet remains an important source of radiation, necessary to account for the BEARS data.

This NLTE modelling shown here does suffer a weakness: it neglects transport from the exobase region upwards. Indeed, a particle having a kinetic energy E=kT at the exobase can reach an altitude located one scale height above the exobase. For example, let’s assume the exobase is located, say, at z_{exo}= 600 km where the gravific acceleration is

$g \sim 9.81 * R_E^2/r_{exo}^2 \sim 8.2$ m s^{-2} and the temperature is T~1000 K. Across small distances, let us neglect variations of g with altitude and write the potential V=m g z. If a particle moves upward with a kinetic energy E= α kT, it can rise up to an altitude such that ΔV= α kT so that Δz = α kT/mg = α H with H the scale height. Replacing g and T by their assumed values and using the atomic oxygen mass, one finds that if α = 1, Δz = H = 63 km. This altitude is reached after a travel time of ~ 125 s and the particle returns freely to the exobase after ~250 s. Similarly, particles having an energy of 6 kT would reach an altitude of ~1000 km (accounting for the decrease of g with altitude) in a time of flight on the order of ~300 s and return to the exobase after ~600 s . These time scales (which neglect the effect of infrequent collisions still occurring in the exosphere) are much smaller than the radiative lifetime of the ground state oxygen sublevels that amount to several hours (~16 h for J=1 and ~3 h for J=0), and it can be guessed that above the exobase, transport will be an important factor that will tend to "project" the nearly LTE distribution of the exobase upward into the exosphere. The real population of the ground state oxygen in the lower exosphere (a few scale heights above the exobase) is thus certainly closer to LTE than what was computed here. Solving the problem in a consistent manner would require the development of a Monte Carlo model coupling the non-themal gas dynamics accounting for photochemistry with the radiative transfer. Such a study is beyond the scope of the present work but the discussion in the above paragraphs suggest that we may expect that the population of the ground state oxygen does remain close to LTE across several scale heights above the exobase.

5. Conclusions

We have modelled the radiative transfer of the OI-98.9 nm multiplet and compared the results with observations from the BEARS sounding rocket and from the STP78-1 satellite. We find that the resonance scattering of 98.9 nm photons of solar origin is a primary photon source that cannot be neglected at high altitude, above ~450 km under high solar activity conditions. We find that the inclusion of a hot oxygen geocorona with a corrected diffusive equilibrium in the exosphere produces an increase of the optical thickness of the medium that allows us to reach a better agreement between the modelled and observed OI-98.9 nm intensity. This increased oxygen density makes little difference to the modelled OI 130.4 nm intensity at high altitude, and no substantial difference to the computed 135.6 nm intensity. Inclusion of resonance scattering of the solar 98.9 nm multiplet, that was not accounted for in previous studies, allows to account for the BEARS sounding rocket measurement at high altitude.

Acknowledgements

This research was supported by the Belgian Fund for Scientific Research (FNRS) grant 1.5093.12 (Crédit aux Chercheurs). B. Hubert is supported by the Belgian Fund for Scientific Research (FNRS), S. Chakrabarti is supported by grants ONR N00014-13-1-0266 and NSF AGS-1315354. This work was supported by the FRFC grant n° 2.4541.11. All data used in this study can be obtained from us on request. The authors thank both reviewers for helpful comments.

References

Ajello, J. M., and D. E. Shemansky (1985), A reexamination of important N_2 cross section by electron impact with application to the dayglow: the Lyman-Birge-Hopfield band system and N I (119.99 nm), *J. Geophys. Res.*, 90, 9845.

Abreu, V. J., A. Dalgarno, J. H. Yee, S. Chakrabarti, and S. C. Solomon (1984), The OI 989-Å Tropical Nightglow, Geophys. Res. Let., 11, 569.

Bates, D.R. (1962). Dielectronic recombination to normal nitrogen and oxygen ions, *Planet. Space. Sci.*, 9, 77.

Bailey, S. M., C. A. Barth, and S. C. Solomon (2002), A model of nitric oxide in the lower thermosphere, J. Geophys. Res., 107, 1205.

Bilitza D. (ed.) (1990), International Reference Ionosphere 1990, NSSDC 90-22, Greenbelt, Maryland.

Bowen, I. S. (1935). The spectrum and composition of gaseous nebulae, *ApJ.*, 81, 1.

Bowyer, S., R. Kimble, F. Paresce, M. Lampton, and G. Penegor (1981), Continuous-readout extreme-ultraviolet airglow spectrometer, *Appl. Opt.*, 20, 477.

Chakrabarti, S., F. Paresce, S. Bowyer, R. Kimble, and S. Kumar (1983), The extreme ultraviolet day airglow, J. Geophys. Res., 88, 4898.

Cotton, D. M. (1991), A study of the terrestrial thermosphere by remote sensing of OI dayglow in the far and extreme ultraviolet, a thesis.

Cotton, D.M., S. Chakrabarti, and G.R. Gladstone (1993a), Preliminary results from the Berkeley EUV airglow rocket spectrometer: OI and N_2 FUV/EUV dayglow in the thermosphere and lower exosphere, *J. Geophys. Res.*, *98*, 21627.

Cotton, D.M., G.R. Gladstone, and S. Chakrabarti (1993b), Sounding rocket observation of a hot atomic oxygen geocorona, *J. Geophys. Res.*, *98*, 21651.

Curdt, W., Brekke, P., Feldman, U., Wilhelm, K., Dwivedi, B.N., Schühle, U., Lemaire, P., 2001. The SUMER spectral atlas of solar-disk features, A&A 375, 591-613, doi: 10.1051/0004-6361:20010364.

De Jager (1964), Solar X-radiation, in Astronomical Observations from Space Vehicles, Steinberg, ed. (Liège, Belgium: Taffin-Lefort), 45.

Feautrier, P. (1964), Sur la résolution numérique de l'équation de transfert, C. R. Acad. Sc. Paris, 258, 3189.

Froese Fischer, C., and H. P. Saha (1983), Multiconfiguration Hartree-Fock results with Breit-Pauli corrections for forbidden transitions in the 2p4 configuration, Phys. Rev. A 28, 3169, DOI:10.1103/PhysRevA.28.3169.

Gérard, J.C., P.G. Richards, V.I. Shematovich and D.V. Bisikalo (1995), The importance of new chemical sources for the hot oxygen geocorona, Geophys. Res. Lett., 3, 279.

Gérard J.-C., B. Hubert, V.I. Shematovich, D.V. Bisikalo, and G.R. Gladstone (2008), The Venus ultraviolet oxygen dayglow and aurora: Model comparison with observations, Planet. Space Sci., 56, 542-552.

Gérard, J.C., B. Hubert, J. Gustin, V.I. Shematovich, D. Bisikalo, G.R. Gladstone and L.W. Esposito (2010)**,** EUV spectroscopy of the Venus dayglow with UVIS on Cassini, Icarus, 211, doi:10.1016/j.icarus.2010.09.020.

Gladstone, G. R., Radiative transfer with partial frequency redistribution in inhomogeneous atmospheres: application to the jovian aurora, J. Quant. Spectrosc. Radiat. Transfer, 5, 545, 1982.

Gladstone, G.R., 1985. Radiative transfer of resonance lines with internal sources. J. Quant. Spectrosc. Radiat. Trans. 33, 453–458.

Gladstone, G.R., 1988. UV Resonance line dayglow emissions on Earth and Jupiter. *J. Geophys. Res.*, 93, 14623.

Hedin, A. E.(1989), Hot oxygen geocorona as inferred from neutral exospheric models and mass spectrometer measurements, J. Geophys. Res., 94, 5523.

Hedin, A. E. (1991), Extension of the MSIS thermosphere model into the middle and lower atmosphere, J. Geophys. Res., 96, 1159.

Hickey, M.P., P.G. Richards and D.G. Torr, New sources for the hot oxygen geocorona: solar cycle, seasonal, latitudinal and diurnal variations, J. Geophys. Res., 100, 17377, 1995.

Hinteregger, H. E., K. Fukui and B. R. Gilson (1981), Observational, reference and model data on solar EUV, from measurements on AE-E, *Geophys. Res. Let.*, 8, 1147.

Hubert B., J.C. Gérard, D.M. Cotton, D.V. Bisikalo , V.I. Shematovich, Effect of hot oxygen on thermospheric O I UV airglow (1999), J. Geophys. Res. (Space Physics), 104, 17139-17143.

Hubert, B.; Gérard, J. C.; Gustin, J.; Shematovich, V. I.; Bisikalo, D. V.; Stewart, A. I.; Gladstone, G. R. (2010), UVIS observations of the FUV OI and CO 4P Venus dayglow during the Cassini flyby, Icarus, 207, 549-557, doi 10.1016/j.icarus.2009.12.029.

Horan, D. M., and R. W. Kreplin (1981), Simultaneous measurements of EUV and soft X-ray solar flare emission, *Solar Physics*, 74, 265

Kella, D., P. J. Johnson, H.B. Pederson, L. Vejby-Christensen and L.H. Anderson (1997), The source of the green light emission determined from a storage ring experiment, *Science, 276*, 1530.

Killen, R., D. Shemansky and N. Mouawad (2009), Expected emission from Mercury's exospheric species, and their ultraviolet-visible signatures, *ApJS.*, 181, 351.

Kreplin R. W.,K.P. Dere, D. M. Horan, and J. F. Meeking (1977), The solar spectrum below 10 Å, In White O.D. (ed), The solar output and its variations, University Press Boulder, 286

Link, R., G. R. Gladstone, S. Shakrabarti, and J. C. McConnell (1988), An analysis of satellite observations of the O I EUV dayglow, *J. Geophys. Res.*, 93, 2693.

Majeed, T.; and Strickland, D. J. (1997), New Survey of Electron Impact Cross Sections for Photoelectron and Auroral Electron Energy Loss Calculations, *J. Phys. Chem. Ref. Data*, 26(2), 335, doi:10.1063/1.556008.

Manson J. E. (1977), Solar spectrum between 10 an 300 Å, In White O.D. (ed), The solar output and its variations, University Press Boulder, 286

Mc Neal, R. J., M. E. Whitson Jr., and G. R. Cook (1974), Temperature dependence of the quenching of vibrationnally excited nitrogen by atomic oxygen, J. Geophys. Res., 79, 1527.

Meier, R. R., D. E. Anderson Jr., L. J. Paxton, R. P. McCoy, and S. Chakrabarti (1987), The OI 3d $^3D^0 - 2p^4\ ^3P$ transition at 1026 Å in the day airglow, *J. Geophys. Res.*, 92, 8767.

Meier, R. R. (1991), Ultraviolet spectroscopy and remote sensing of the upper atmosphere, *Space Sci. Rev.*, *58*, 1.

Mihalas, D. (1978), Stellar atmospheres, second edition, W.H. Freeman Company, San Francisco, USA.

Moore, C.E. (1993), Tables of Spectra of Hydrogen, Carbon, Nitrogen, and Oxygen Atoms and Ions, in CRC Series in Evaluated Data in Atomic Physics, 339 pp. (Ed. J. W. Gallagher, CRC Press, Boca Raton, FL, 1993)

Nagy, A. F., and P. M. Banks (1970), Photoelectron fluxes in the ionosphere, *J. Geophys. Res.*, 75, 6260.

Péquignot D. (1990), Populations of the O I metastable levels, *Astron. Astrophys.*, 231, 499

Reader, J., C. H. Corliss, W. L. Wiese, and G. A. Martin (1980), Wavelengths and transition probabilities for atoms and atomic Ions, part. I. Wavelengths, Part II. Transition probabilities, *Nat. Stand. Ref. Data Ser.*, NSRDS-NBS 68

Rees, M. H. (1989.), Physics and chemistry of the upper atmosphere, Cambrige University Press, Cambrige.

Richards, P. G., M. P. Hickey and D. G. Torr (1994a), New sources for the hot oxygen geocorona, *Geophys. Res. Lett., 21*, 657.

Richards, P. G., J. A. Fenelly and D. G. Torr (1994b), EUVAC: A solar EUV flux model for aeronomic calculations, *J. Geophys. Res.*, 99, 8981.

Roble, R. G. (1995), Energetics of the mesosphere and thermosphere, in The upper mesosphere and lower thermosphere, Geophysical Monograph Series, 87, edited by R. M. Johnson and T. L. Killeen, AGU, Washington D. C..

Sharma, R., B. Zygelman, F. von Esse, and A. Dalgarno (1994), On the relationship between the population of the fine structure levels of the ground electronic state of atomic oxygen and the translational temperature, *Geophys. Res. Lett.*, 21, 1731.

Shematovich V.I., D.V. Bisikalo, J.C. Gérard (1994), A kinetic model of the formation of the hot oxygen geocorona. 1. Quiet geomagnetic conditions, *J. Geophys. Res., 99*, 23217.

Shizgal, B., and M. J. Linderfeld, Further studies of non-Maxwellian effects associated with the thermal escape of a planetary atmosphere, *Planet. Space. Sci., 28*, 159, 1980.

Siskind, David E.; Strickland, D. J.; Meier, R. R.; Majeed, T.; Eparvier, F. G. (1995), On the Relationship Between the Solar Soft X Ray Flux and Thermospheric Nitric Oxide: An Update with an Improved Photoelectron Model, *J. Geophys. Res.*, 100, 19687, doi:10.1029/95JA01609.

Smith, E. V. P. and D. M. Gottlieb (1974), Solar flux and its variations, *Space Sci. Rev.*, 16, 771.

Solomon S. C., P. B. Hays and V. Abreu (1988), The auroral 6300 Å emission : observation and modeling, *J. Geophys. Res.*, *93*, 9867.

Solomon, S. C., and V. J. Abreu (1989), The 630 nm dayglow, J. Geophys. Res., 94, 6817.

Solomon, S. C. (2001), Auroral particle transport using Monte Carlo and hybrid methods, J. Geophys. Res., 106, 107.

Solomon, S. C., S. M. Bailey, and T. N. Woods (2001), Effect of solar soft X-rays on the lower atmosphere, Geophys. Res. Lett., 28, 2149.

Strickland, D. J.; Evans, J. S.; Paxton, L. J (1995), Satellite Remote Sensing of Thermospheric O/N2 and solar EUV, 1. Theory, *J. Geophys. Res.*, 10, 12217, doi:10.1029/95JA00574.

Strickland, D. J.; Majeed, T.; Evans, J. S.; Meier, R. R.; Picone, J. M. (1997), Analytical representation of g factors for rapid, accurate calculation of excitation rates in the dayside thermosphere, *J. Geophys. Res.*, 102, 14485, doi:10.1029/97JA00943.

Strickland, D. J., J. Bishop, J.S. Evans, T. Majeed, P.M. Shen, R.J. Cox, R. Link, R.E. Huffman (1999), Atmospheric Ultraviolet Radiance Integrated Code (AURIC): theory, software architecture, inputs, and selected results, *JQSRT*, 62, 689, doi:10.1016/S0022-4073(98)00098-3.

Swaminathan, P. K.; Strobel, D. F.; Kupperman, D. G.; Kumar, C. Krishna; Acton, L.; DeMajistre, R.; Yee, J.-H.; Paxton, L.; Anderson, D. E.; Strickland, D. J.; Duff, J. W. (1998), Nitric oxide abundance in the mesosphere/lower thermosphere region: Roles of solar soft X rays, suprathermal N(4S) atoms, and vertical transport, *J. Geophys. Res.*, 103, 11579, doi:10.1029/97JA03249.

Tinsley, B. A., and A. B. Christensen (1973), Excitation of oxygen permitted line emission in the tropical nightglow. *J. Geophys. Res.*, 78, 1174.

Tobiska, W.K. (2004), SOLAR2000 irradiances for climate change, aeronomy and space system engineering. Adv. Space. Res. 34. 1736–1746.Torr, M. R., D. G. Torr, P. G. Richards, and S. P. Yung (1990), Mid- and low- latitude model of thermospheric emission 1. O+(2P) 7320 Å and N2(2P) 3371 Å, J. Geophys. Res., 95, 21147.

Wagner, W. J. (1988), Observations of 1–8 Å solar X-ray variability during solar cycle 21, *Adv. Space Res.*, 8, 67.

Wiese, W. L., J. R. Fuhr, and T. M. Deters, (1996), Atomic transition probabilities of carbon, nitrogen, and oxygen – A critical data compilation, J. Phys. Chem. Ref. Data, Monograph No. 7, AIP Press, Melville, NY, 532 pp.

Woods, T., Rottman, G. (2002), Solar ultraviolet variability over time periods of aeronomic interest, atmospheres in the solar system: comparative aeronomy. In: Mendillo, M., Nagy, A., Waite, J.H. (Eds.), Geophysical Monograph 130. American Geophysical Union, Washington, DC, p. 221 - 234.

Yee, J. H., J.W. Meriwether, and P.B. Hays (1980), Detection of a corona of fast oxygen atoms during solar maximum, *J. Geophys. Res.*, *85*, 3396.

Zygelman B., A. Dalgarno and R.D. Sharma (1994), Excitation of the $^3P_{J=0,1,2}$ fine structure of atomic oxygen in collisions with oxygen atoms, *Phys. Rev. A*, 50,3920

Tables.

Reaction	Reaction coefficient ($cm^{-3}\ s^{-1}$)		ΔE (eV)
$NO^+ + e \rightarrow N + O$	$4.3\times10^{-7}(T_e/300)^{-1}$	(22%)	2.75
$NO^+ + e \rightarrow N(^2D) + O$	$4.3\times10^{-7}(T_e/300)^{-1}$	(78%)	0.38
$O_2^+ + e \rightarrow O + O$	Torr et al. [1990] (FLIP model)		4.42
$O + N(^2D) \rightarrow N(^4S) + O$	$\sim 7\times10^{-13}$		2.38
$O + O(^1D) \rightarrow O + O$	8×10^{-12}		1.96
$O + O^+(^2P) \rightarrow O^+ + O$	4×10^{-10}		5.00
$O+O^+(^2D) \rightarrow O^+ + O$	5×10^{-12}		3.31
$N(^2D) + O^+ \rightarrow N^+ + O$	5×10^{-11}		1.46
$O_2 + O^+ \rightarrow O_2^+ + O$	$2.1\times10^{-11}\ (T_n + 2\ T_i/3\times300)^{-0.763}$		1.55
$N_2 + O^+(^2D) \rightarrow N_2^+ + O$	8×10^{-10}		1.33
$O(^1D) + N_2 \rightarrow O + N_2$	$2.0\times10^{-11}\exp(107.8\ \ T)$		1.96
$O^+ + H \rightarrow O + H^+$	$2.2\times10^{-11}\ T^{0.5}$		kT_i
$N(^2D) + O_2 \rightarrow NO + O$	6×10^{-12}		3.76
$N(^2P) + O \rightarrow N + O$	1.7×10^{-11}		3.58
$NO + N \rightarrow N_2 + O$	3.4×10^{-11}		3.25
$N(^4S) + O_2 \rightarrow NO + O$	$4.4\times10^{-12}\ \exp(-3220/T)$		1.385
$N^+ + O_2 \rightarrow NO^+ + O$	2×10^{-10}		6.67
$O^+(^2D) + O_2 \rightarrow O_2^+ + O$	7×10^{-10}		4.865
$O^+(^2P) + N_2 \rightarrow N_2^+ + O$	4.8×10^{-10}		3.02
$O(^1D) + O_2 \rightarrow O_2 + O$	$2.9\times10^{-11}\ \exp(67.5/T)$		1.96
$O_2^+ + N \rightarrow NO^+ + O$	1.2×10^{-10}		4.2
$NO + N(^2D) \rightarrow N_2 + O$	7×10^{-11}		5.63
$N_2^*(v = i) + O \rightarrow N_2(v' = i\text{-}1) + O$	M^c Neal et al. [1974]		

Table 1. Important exothermal reaction processes producing fast oxygen atoms, with their reaction coefficients and exothermicity ΔE (after Richards et al. [1994]).

$F_{10.7}$	a x 10^2	b x 10^3	β_0 x 10^2	T_h (K)
70	0.790	2.934	0.729	10644
200	1.064	2.564	1.048	10487

Table 2. Fitting parameters obtained for the hot versus thermal ratio of equation (2) under solar minimum and maximum conditions.

Feature	λ (nm)	g_l	g_u	A_{ul} (s^{-1})	ω_0
O I (135.6 nm)	135.5598	5	5	4.20(3)	1
$^3P_{2,1} \leftarrow {}^5S^o_2$	135.8512	3	5	1.36(3)	1
O I (130.4 nm)	130.2168	5	3	3.41(8)	1
($^3P_{2,1,0} \leftarrow {}^3S^o_1$)	130.4858	3	3	2.03(8)	1
	130.6029	1	3	6.76(7)	1
O I (102.7 nm)	102.5762	5	3	2.11(6)	0.7433
$^3P_{2,1,0} \leftarrow$ 3d $^3D^o_{3,2,1}$	102.7431	3	3	3.17(7)	0.7433
	102.8157	1	3	4.22(7)	0.7433
	102.5762	5	5	1.91(7)	0.7112
	102.7431	3	5	5.71(7)	0.7112
	102.5762	5	7	7.66(7)	0.7106
O I (98.9 nm)	98.8578	5	3	6.47(6)	0.99953
$^3P_{2,1,0} \leftarrow$ 3s' $^3D^o_{3,2,1}$	99.0127	3	3	9.47(7)	0.99953
	99.0801	1	3	1.25(8)	0.99953
	98.8655	5	5	5.77(7)	0.99975
	99.0204	3	5	1.68(8)	0.99975
	98.8773	5	7	2.26(8)	0.99972

Table 3. Transition parameters of the oxygen FUV and EUV multiplets. Read 4.20(3) as 4.20 x 10^3. The degeneracies are computed from the angular momentum quantum number (g = 2 J + 1). The lines multiplets are separated in sub-multiplets according to their upper substates, that can be identified from the degeneracy g_u. The single scattering albedos used in our simulations are given in the last column, based on the Einstein transition parameters of the branching transitions and those listed here. All numbers are from Reader et al. [1980] and Wiese et al. [1996] and can be easily found on the NIST web site.

FIGURES.

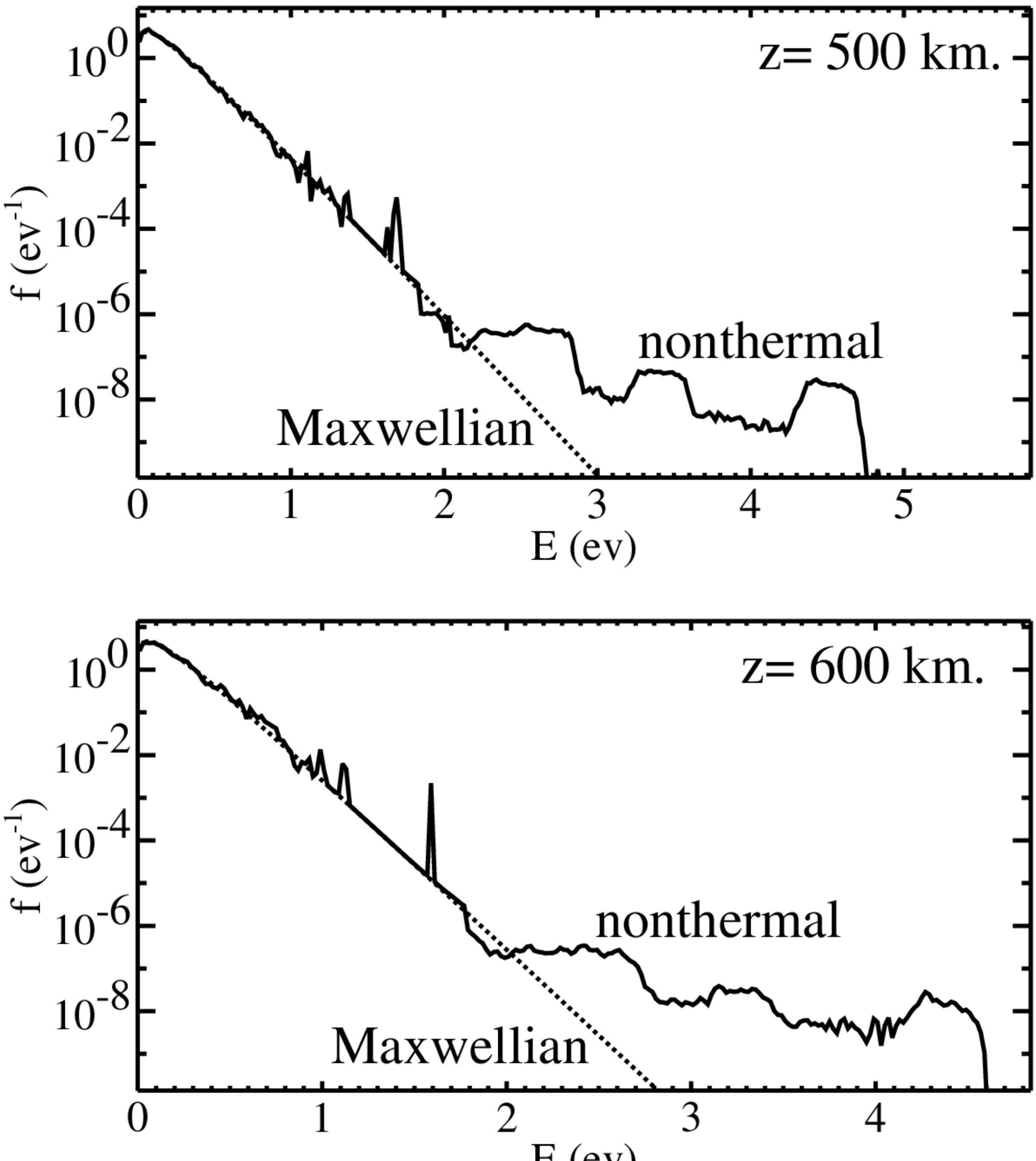

Figure 1. Oxygen distribution functions computed at 500 and 600 km under high solar activity. Solid lines represent the Monte Carlo simulation results, while the dotted lines show the Maxwellian distribution function at the temperature predicted by the MSIS model. The superthermal population consists in the small disturbances found near E = 1 eV.

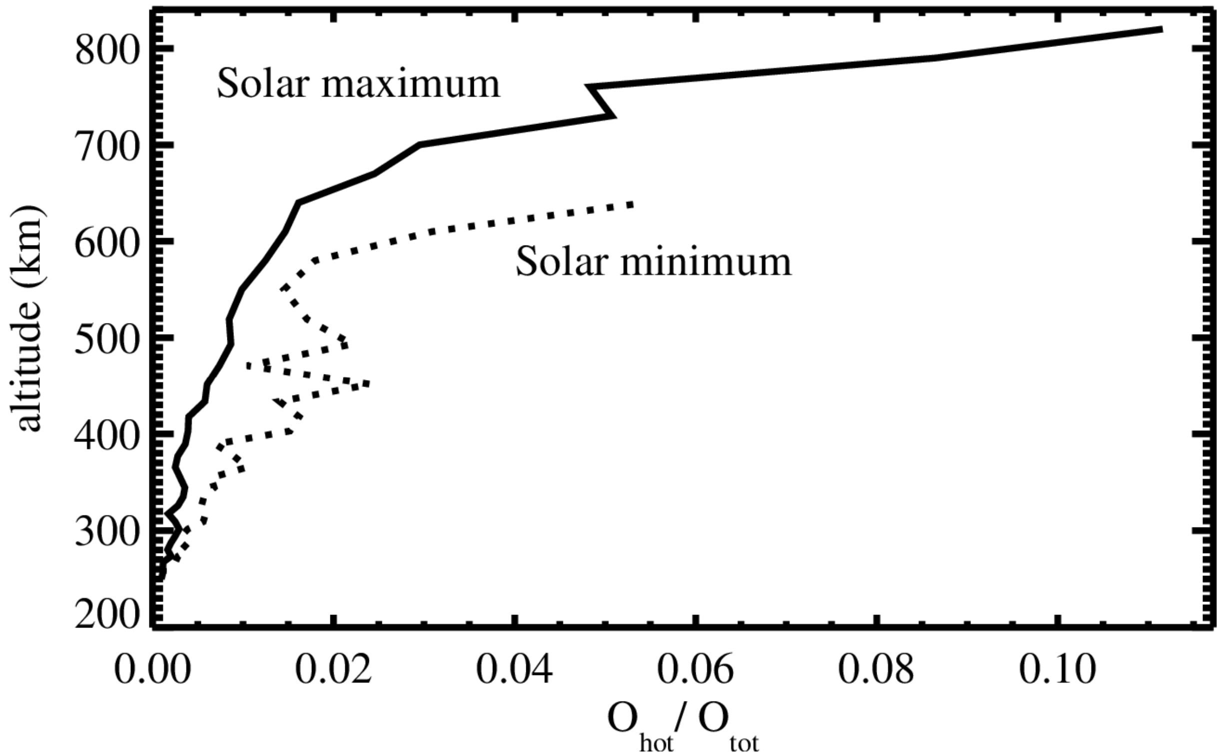

Figure 2. Ratio of the computed superthermal, hot, oxygen density over the total oxygen density, computed under solar minimum and solar maximum conditions.

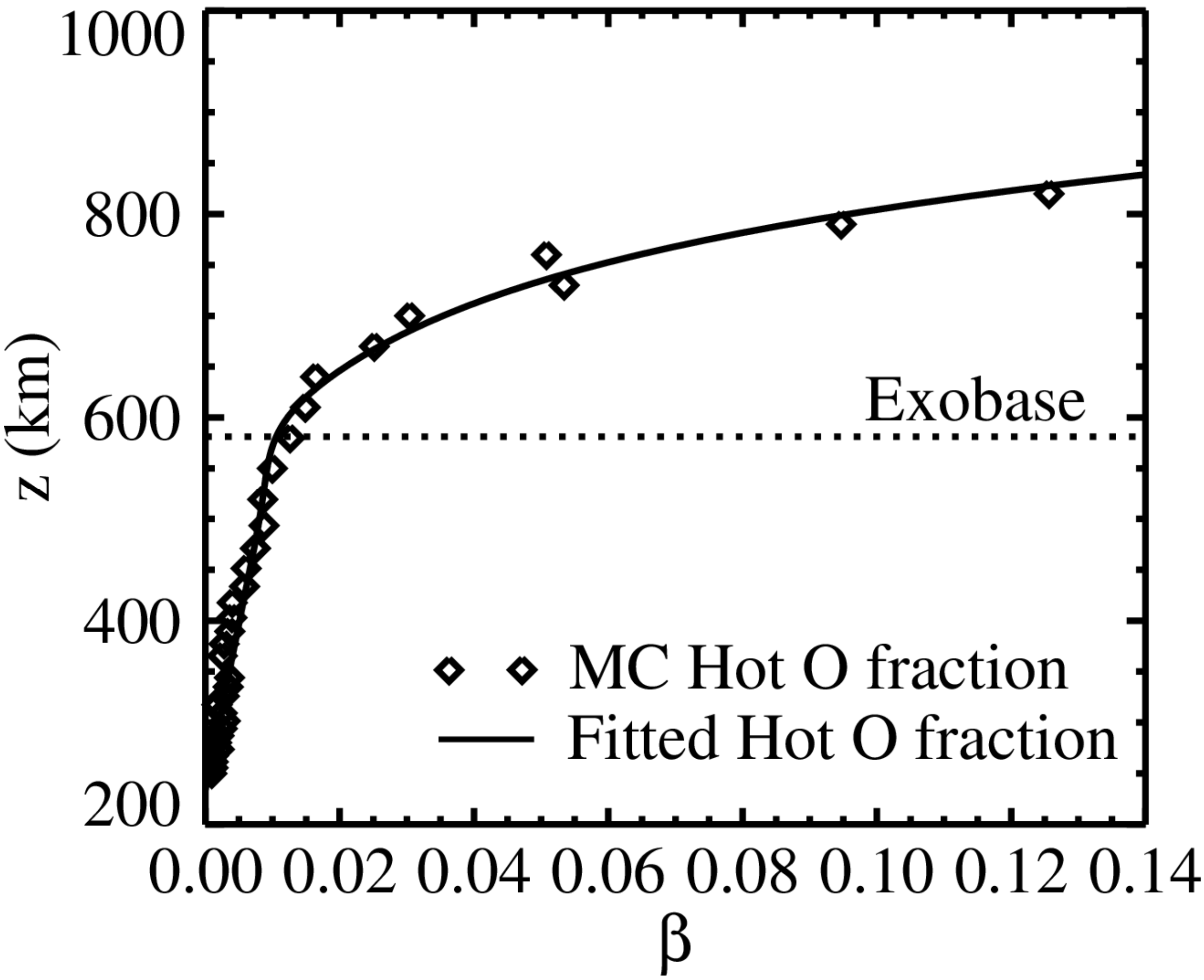

Figure 3. Fraction of superthermal oxygen atoms computed under maximum solar activity (diamonds) and fitted using the function of equation 2 (solid line). The horizontal dotted line shows the altitude of the exobase.

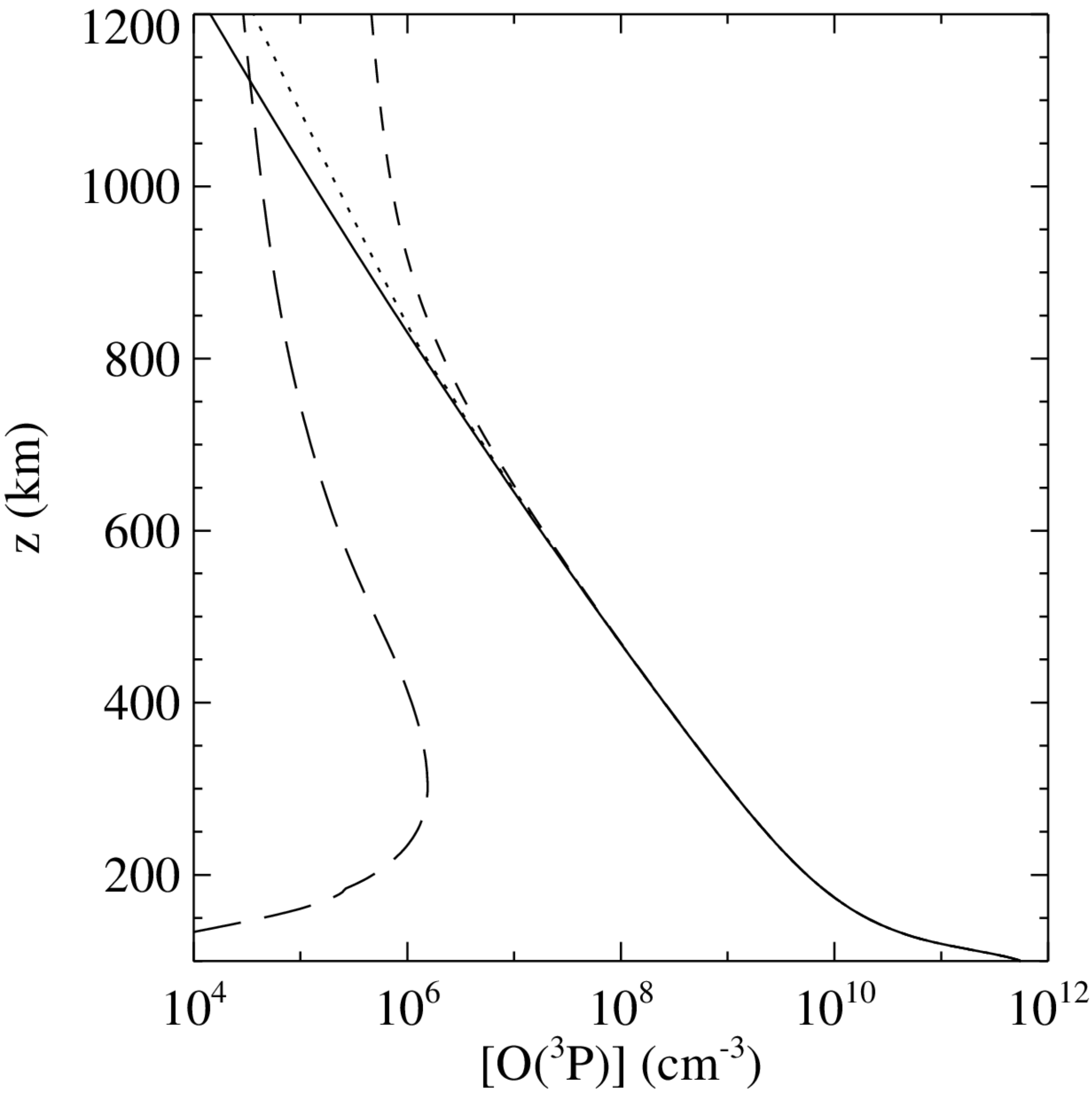

Figure 4. Oxygen density profile from the MSIS-90 model (solid line), with a diffusive correction accounting for the presence of a hot oxygen component (dotted line) and assuming that the thermal and non-thermal oxygen components follow separate diffusive equilibrium profiles above the exobase (dashed line). The long dashes represent the O^+ concentration.

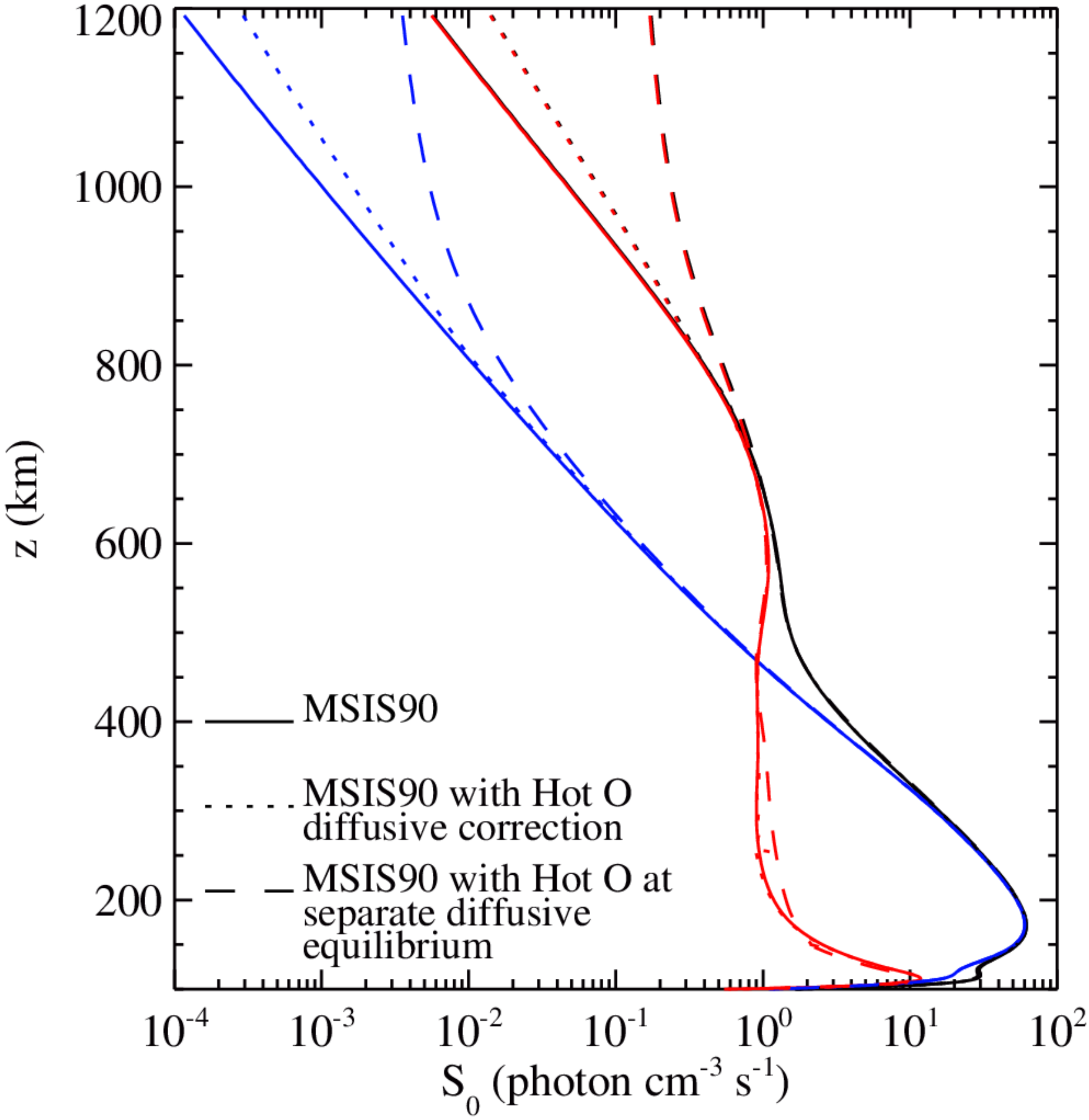

Figure 5. Primary source of 98.9 nm photons computed using the MSIS90 atmosphere(solid line); MSIS90 atmosphere corrected at diffusive equilibrium for the presence of the hot oxygen population (dotted line), and summing the MSIS90 oxygen density with the hot O density at separate diffusive equilibrium (dashed line). Blue lines show the photochemical sources, red lines show the resonance scattering of the solar photons, black lines show the total. The solar contribution to the primary source becomes dominant around 450 km.

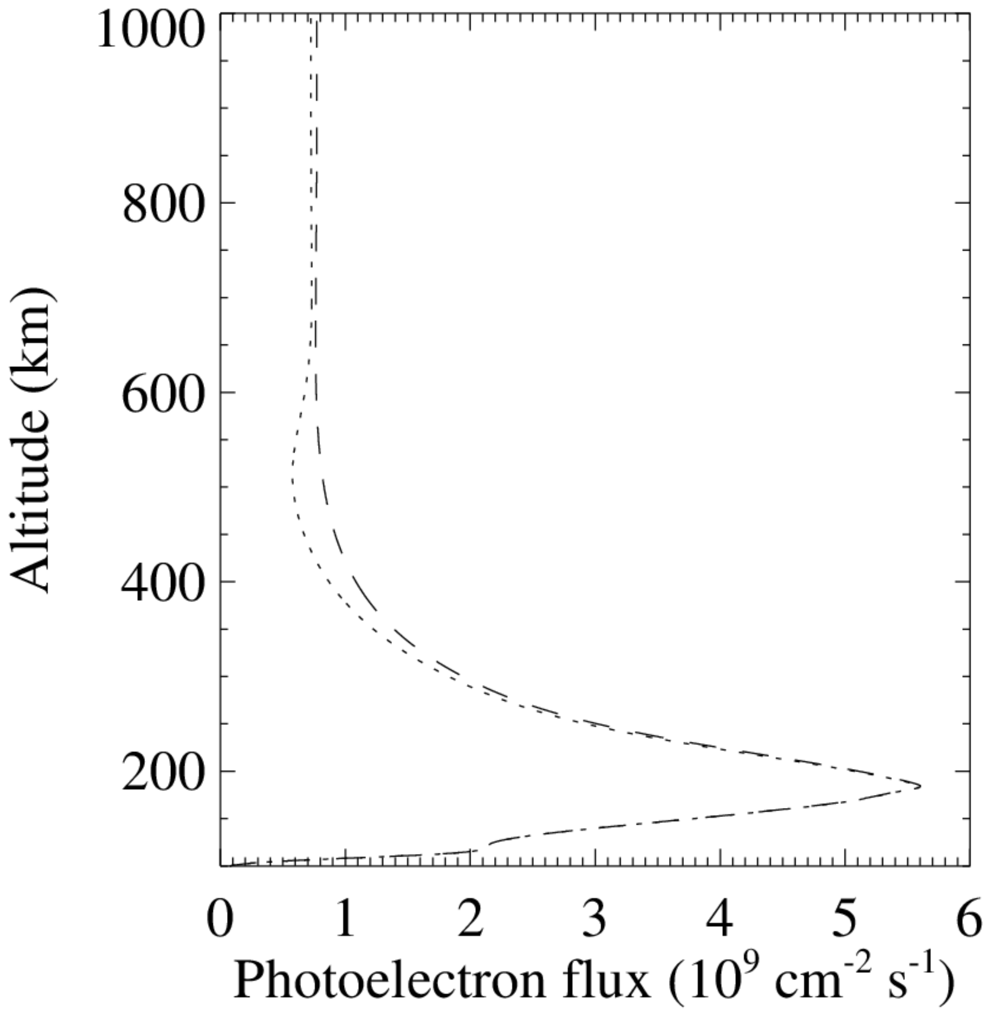

Figure 6. Upward (dashed line) and downward (dotted line) photoelectron fluxes computed using the glow model without any hot oxygen correction to the atmosphere of the MSIS90 model, for the conditions prevailing when the BEARS sounding rocket was launched.

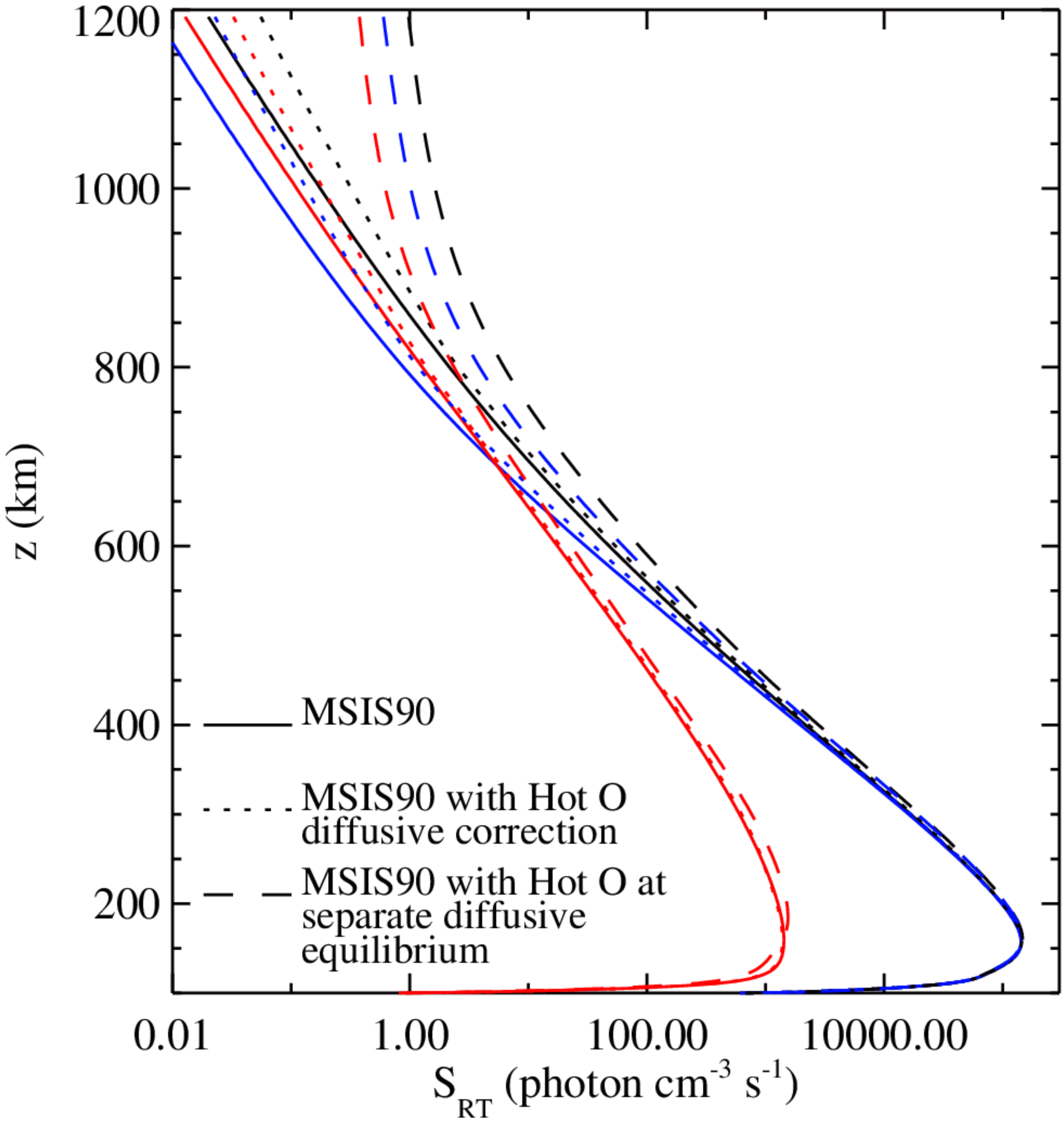

Figure 7. Radiative transfer source function of the OI 98.9 nm multiplet computed using the MSIS90 atmosphere (solid lines); MSIS90 atmosphere corrected at diffusive equilibrium for the presence of the hot oxygen population (dotted lines), and summing the MSIS90 oxygen density with the hot O density at separate diffusive equilibrium (dashed lines). Blue lines show the photochemical sources, red lines show the resonance scattering of the solar photons, black lines show the total.

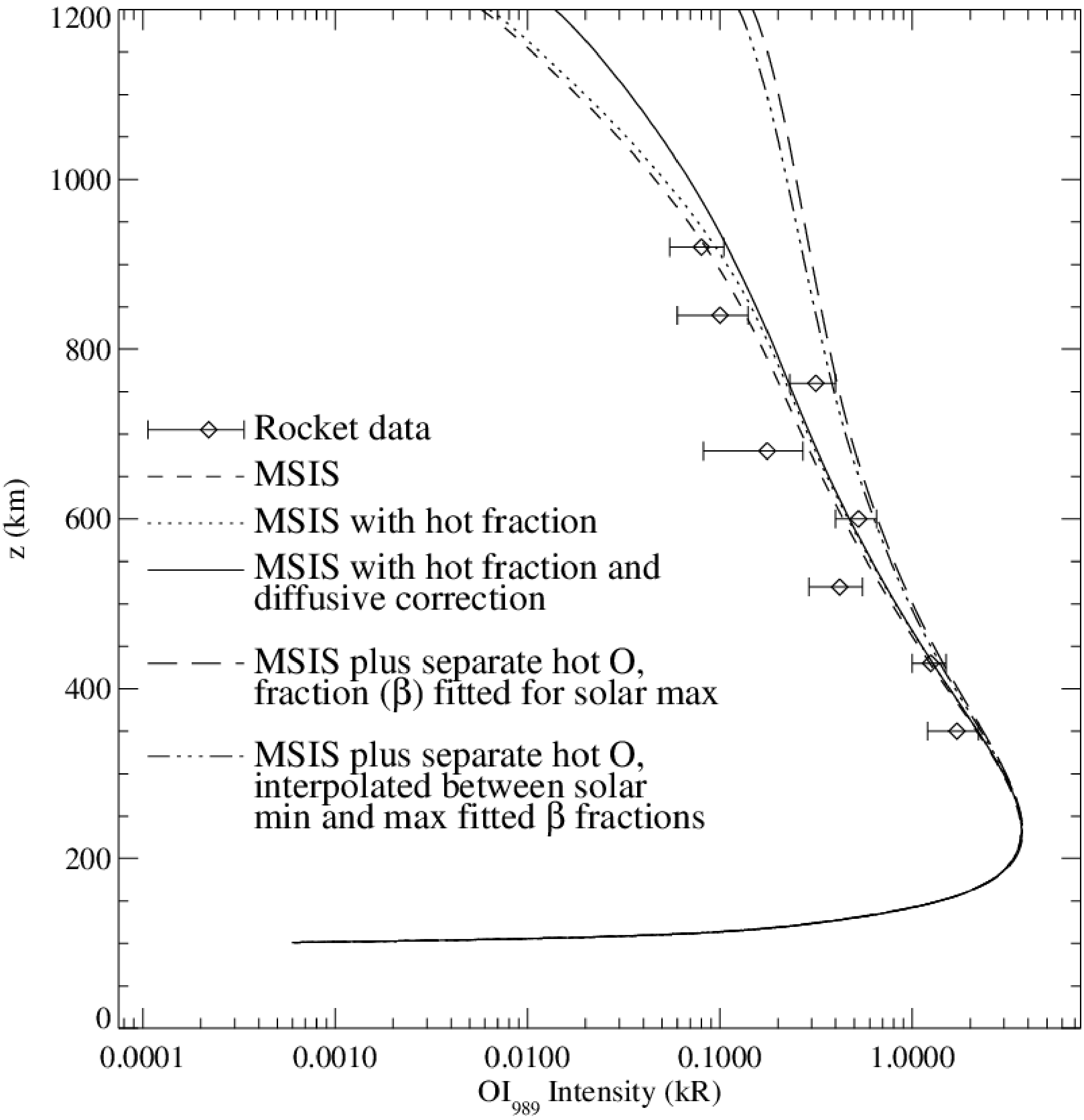

Figure 8. OI 98.9 nm multiplet intensity measured during the BEARS sounding rocket launch (diamonds) and modeled using the MSIS90 atmosphere (short dashes), the MSIS90 oxygen total density with a hot oxygen fraction as computed with the Monte Carlo model (dotted lines), the MSIS90 oxygen profile corrected at diffusive equilibrium to account for the hot oxygen population (solid lines), the MSIS90 oxygen density increased by the hot oxygen population at separate diffusive equilibrium according to the Monte Carlo computation under solar maximum conditions (long dashes) and the MSIS90 oxygen density increased by the hot oxygen population interpolated versus $F_{10.7}$ using the solar minimum and solar maximum Monte Carlo simulations (dash-dot lines).

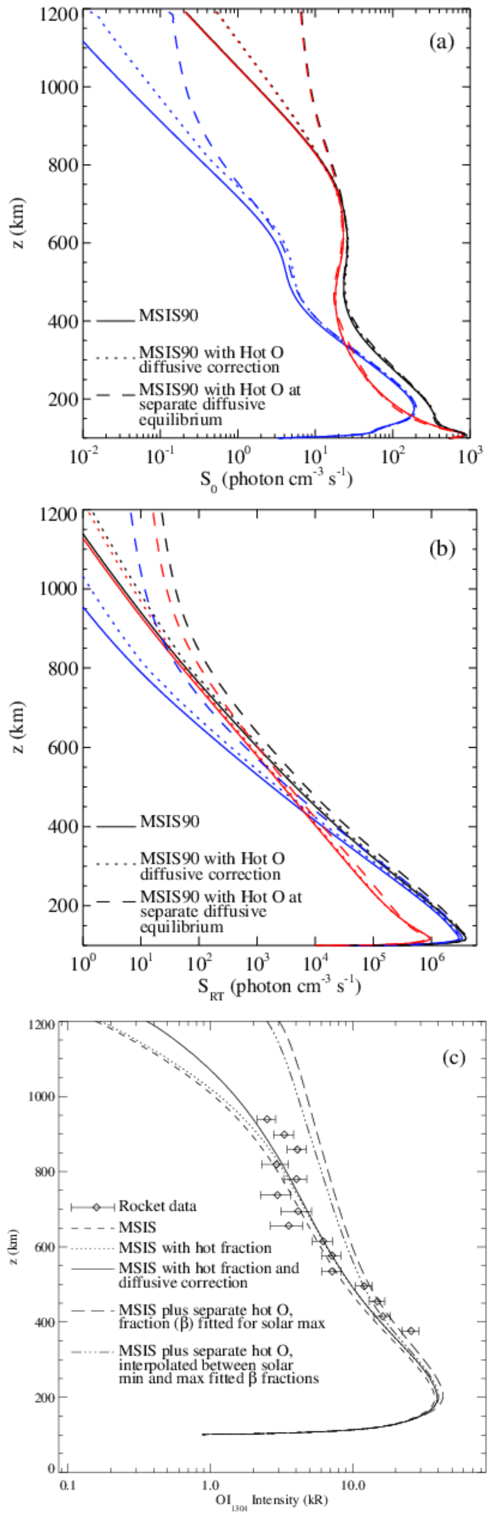

Figure 9. Primary source function (a), optically thick source function (b) and intensity (c) of the 130.4 nm oxygen triplet. Plotting conventions are identical to those of figures 5, 7 and 8.

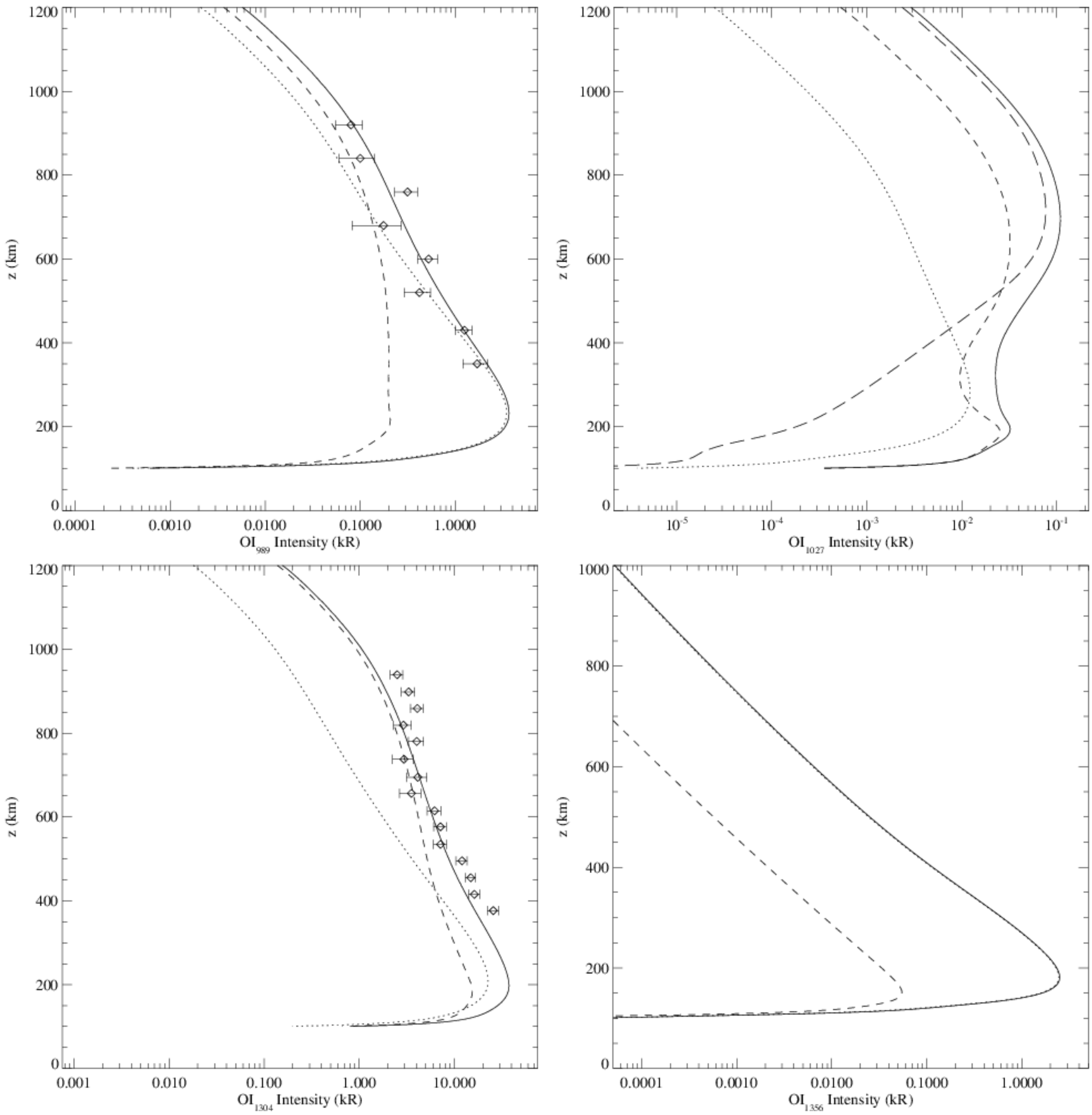

Figure 10. Vertical profile of the intensity of the OI 98.9, 102.7, 130.4 and 135.6 nm multiplets. The dotted (dash) lines represent the contribution from the photochemical sources (from the scattering of the solar multiplet, respectively). For the 120.7 nm multiplet, the long dashes represent the contribution due to the scattering of the solar Lyman-α. The solid lines represent the total. The diamonds show the BEARS data, obtained at 98.9 and 130.4 nm.

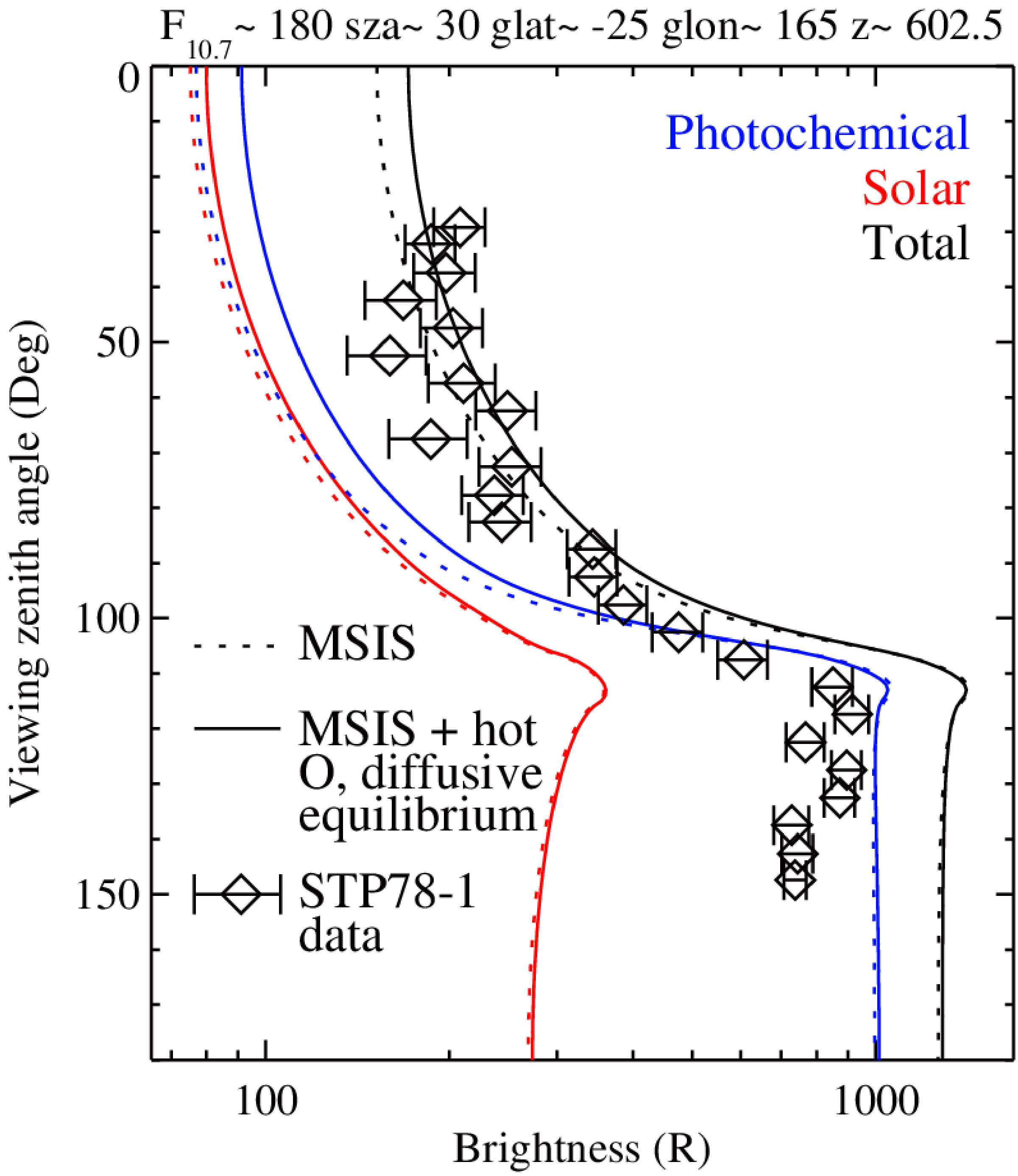

Figure 11. Oxygen 98.9 nm intensity measured by the STP78-1 satellite on March 21 1979. Data obtained during 10 rotations of the satellite (angular scans) were accumulated, according to geographical selection criteria: the latitude of the viewing tangent height was located between -20° and -30°, the longitude between 160° and 170°, and the solar zenith angle between 20° and 40°. The radiative transfer computed brightness is also shown. Red lines represent the contribution of the resonantly scattered solar photons entering radiative transfer, the blue lines show the contribution of the photochemical sources of photons, the black curves represent the total. Dotted lines show the brightness computed using the MSIS90 atmosphere. Solid lines show the brightness computed including the hot oxygen population and correcting the total density accordingly applying diffusive equilibrium.

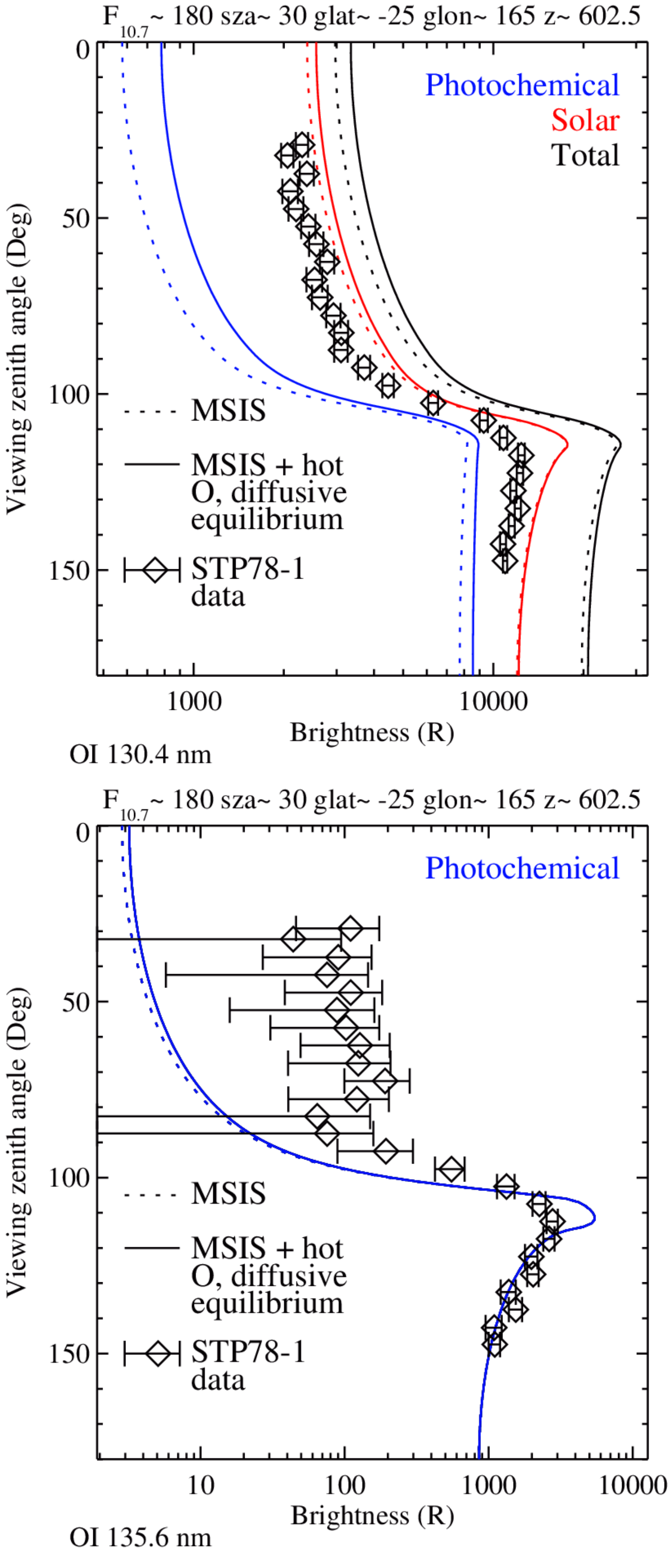

Figure 12. OI 130.4 and 135.6 nm intensities measured by the STP78-1 satellite on 21 March 1979 at daytime. Data obtained during 10 rotations of the satellite (angular scans) were

accumulated, according to geographical selection criteria: the latitude of the viewing tangent height was located between -20° and -30°, the longitude between 160° and 170°, and the solar zenith angle between 20° and 40°. The 130.4 nm radiative transfer computed brightness is also shown (upper panel). Red lines represent the contribution of the resonantly scattered solar photons entering radiative transfer, the blue lines show the contribution of the photochemical sources of photons, the black curves represent the total. Dotted lines show the brightness computed using the MSIS90 atmosphere. Solid lines show the brightness computed including the hot oxygen population and correcting the total density accordingly applying diffusive equilibrium. The simulated OI 135.6 nm intensity is also shown (lower panel)

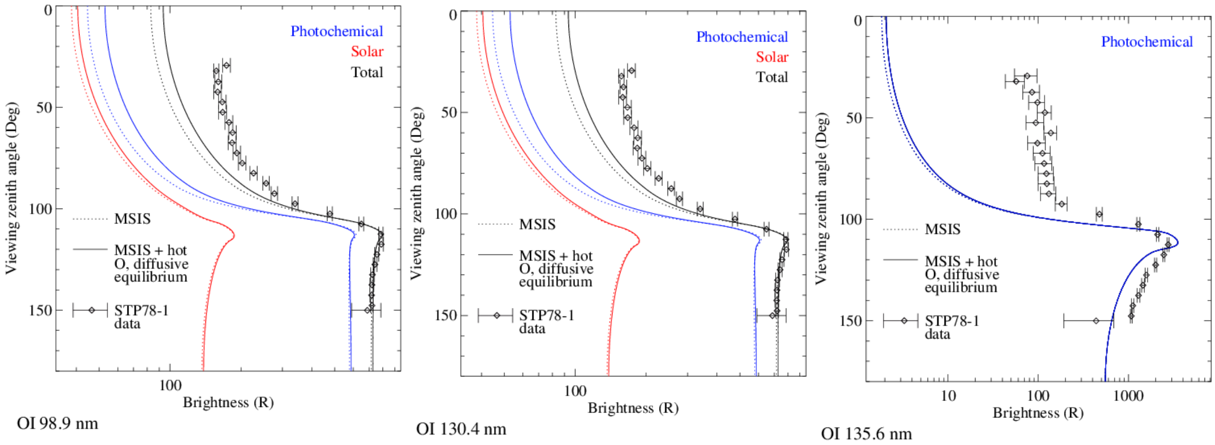

Figure 13. Dayglow intensity measured by the STP78-1 satellite on 21 March 1979 at 98.9 nm (left panel), 130.4 nm (middle panel) and 135.6 nm (right panel), average on two orbits. The average modeling of these emissions is also shown (black curves) detailing the contributions of photochemical origin (blue curves) and solar origin (red curves). Dotted lines represent simulations realized using the MSIS90 atmosphere, solid curves account for the presence of the superthermal oxygen population assumed and correcting the total density accordingly applying diffusive equilibrium. A scaling factor is applied to the modeled total intensities to fit the observed brightness in a least squares sense (for look zenith angles larger than 100°).

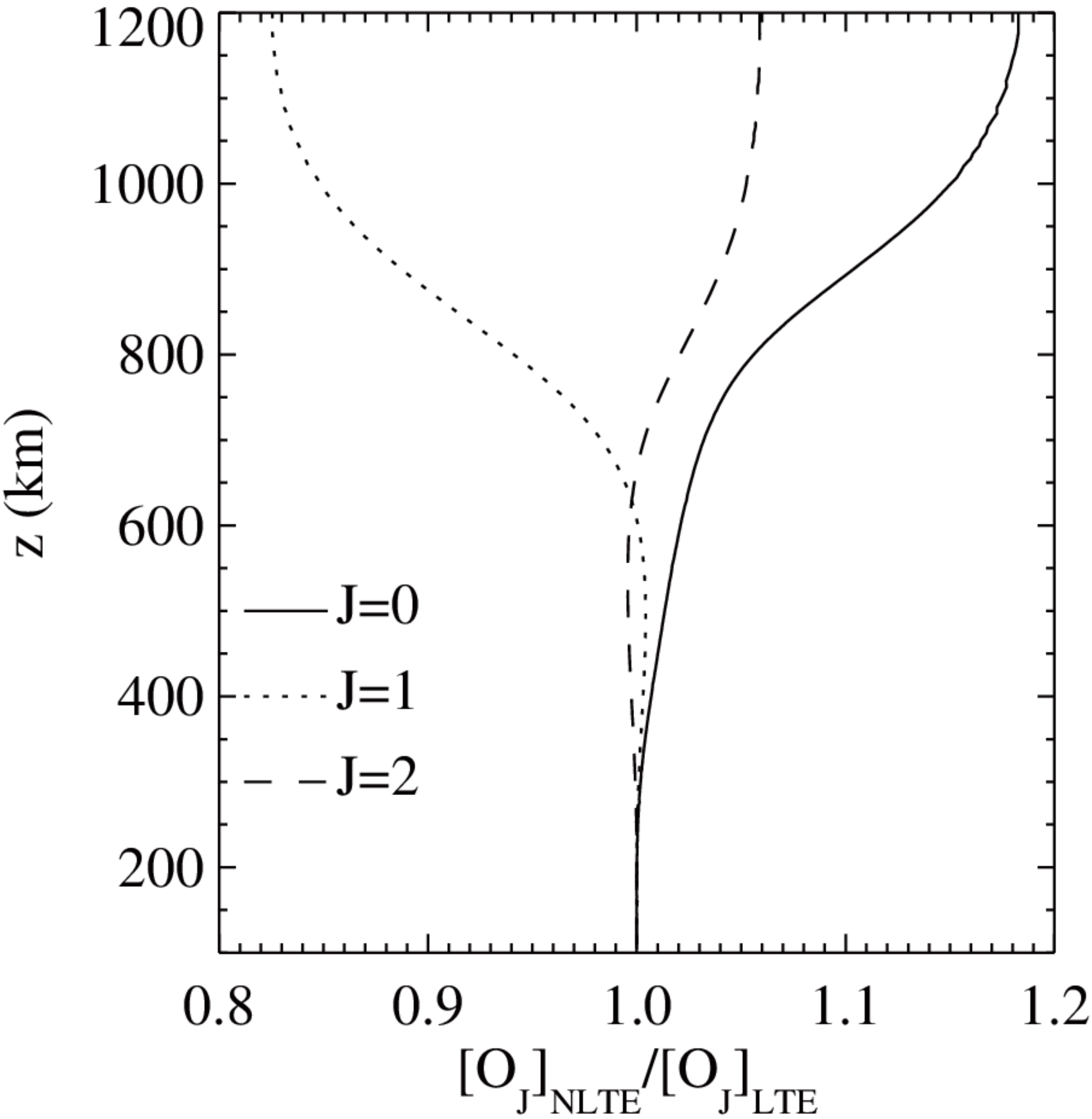

Figure 14. Ratio between the non-LTE and LTE populations of the ground state oxygen sublevels, obtained assuming the atmosphere is given by the MSIS model, the ionosphere by the IRI model and accounting for the effect of UV radiative transfer.

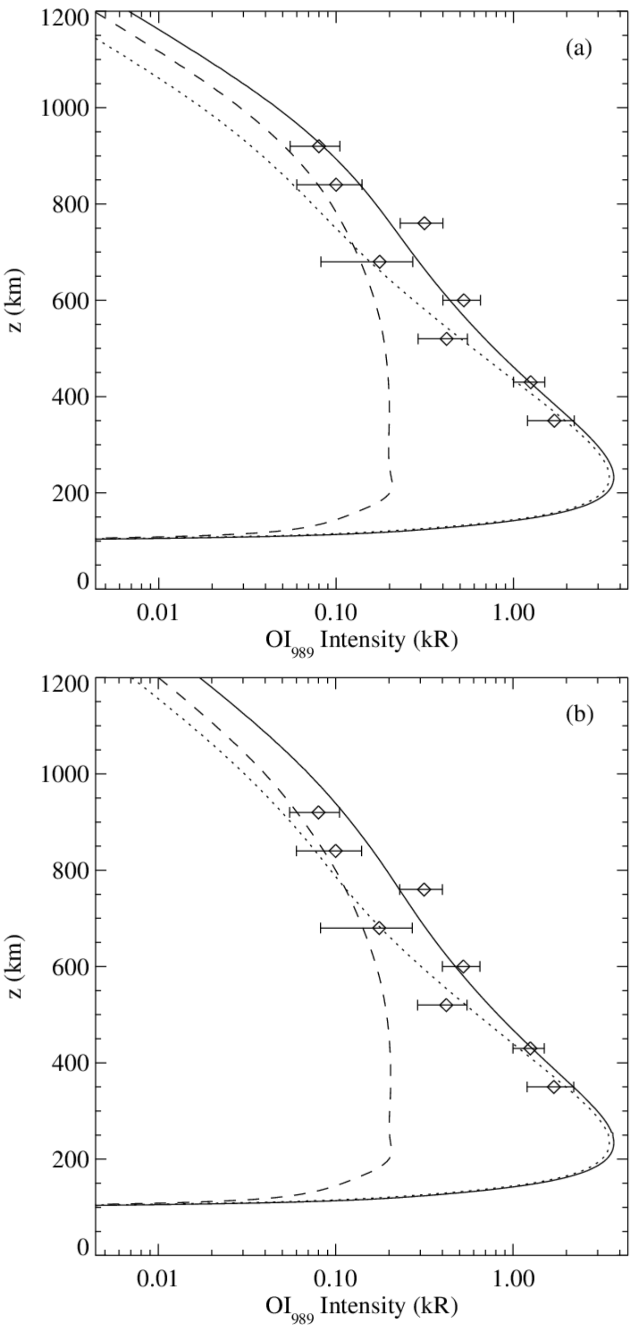

Figure 15. OI 98.9 nm intensity profile computed under the conditions of the BEARS sounding rocket launch applying an NLTE population of the ground state oxygen atoms consistent with the computed UV radiation field. The MSIS atmosphere is used in panel a, while atomic oxygen has a nonthermal energy distribution in panel b and the diffusive density profile is corrected accordingly. Dotted (dashed) lines represent the intensity resulting from the photochemical sources of radiation (from the scattering of the solar 98.9 multiplet, respectively) and the solid line is the total. The diamonds represent the BEARS observation.